Cite as: Zhu, T., Yu, B., Silva-Lopez, R., and Baker, J. W. (2026). Simulating dynamic transport-economic interdependencies for post-earthquake regional economic recovery. *Reliability Engineering & System Safety*, 113700.
DOI: https://doi.org/10.1016/j.ress.2026.113700
This is the authors' accepted manuscript. The final published version is available at the DOI above.

Simulating dynamic transport-economic interdependencies for post-earthquake regional economic recovery

Tinger Zhu[1,*], Bofan Yu[1], Rodrigo Silva-Lopez[1], Jack W. Baker[1]

Abstract

Infrastructure disruptions from natural hazards can generate substantial indirect economic losses through complex, time-dependent interdependencies between physical systems and regional economies. Systematic quantification of these propagation mechanisms is essential for developing actionable mitigation and recovery strategies that maximize societal benefits. This study develops a dynamic modeling framework that explicitly links transport system disruptions, including road networks and ports, to regional economic performance through physical constraints on labor and freight mobility. The framework integrates hazard simulation, physical system damage and recovery modeling, and a refined Adaptive Regional Input–Output (R-ARIO) model to dynamically simulate sectoral economic activities as physical disruptions evolve over time. We apply the framework to evaluate the indirect economic impacts of transport system disruption in the San Francisco Bay Area under a magnitude 7.3 Hayward earthquake scenario. Besides the direct building damage of $47.9 billion, the model estimates that transport system disruption can generate an additional $3.3 billion indirect economic loss on top of the $62.3 billion indirect loss attributed to building damage. Road network and port disruptions exhibit distinct temporal effects on regional economic performance, with varying sensitivities across economic sectors. Moreover, the physics-based integration enables the identification of sector-specific bottlenecks and associated critical periods introduced by each transport system during recovery, providing actionable insights for targeted mitigation and resilience planning to reduce cascading economic impacts.

Keywords: Indirect economic impacts, System interdependencies, Recovery trajectory simulation

1. Introduction

Disaster resilience for infrastructure systems has implications that extend beyond engineering concerns of physical damage and service reliability to broader socioeconomic stability for communities. The interdependencies between infrastructure and economic systems can exacerbate the disaster-induced losses and

[1]Department of Civil and Environmental Engineering, Stanford University, Stanford, California, U.S.A.
[*]Corresponding author. Email: zhut@stanford.edu

socioeconomic disruptions. In particular, transport systems are critical for the functionality of economic systems both during and after disasters [1]. For example, the 1994 Northridge earthquake damaged major freeways and arterials in Los Angeles, causing more than $1.5 billion business interruption loss [2]. The 1995 Kobe earthquake resulted in the closure of the Port of Kobe for nearly two years, triggering employment losses and traffic diversions that amounted to $4 billion in the first three quarters following the event [3]. The 2010–2011 Canterbury earthquakes likewise caused extensive damage to tunnels, bridges, ports, and airports, disrupting freight, shipping, and air transport [4]. While the importance of accounting for infrastructure disruptions in building community resilience is increasingly recognized in public policy [5], ongoing efforts continue to develop methodologies for systematically assessing these impacts and translating modeling results into actionable mitigation and recovery strategies.

Understanding indirect impacts of transport infrastructure disruptions requires modeling methods for both functionality assessment of physical infrastructure and economic analysis to quantify downstream consequences. Transport systems are composed of interconnected components, and disruptions to individual elements can generate cascading impacts within the system. Functional assessments typically evaluate component-level vulnerability and translate it into system-level performance degradation. For ports, system-level impacts are often quantified in terms of remaining operational capacity [6, 7] or lost revenue [8, 9]. For road networks, commonly used performance metrics include travel time/distance, throughput and accessibility [10]. Some studies extend the analysis by incorporating the social costs of disrupted mobility. For instance, Zhou et al. [11] estimate opportunity costs based on trip purposes, Postance et al. [12] derive losses from market values of occupant time and vehicle operation, Silva-Lopez et al. [13] evaluate welfare losses due to travel delays, and Boakye et al. [14] assess the capability loss of individuals from disrupted connectivity.

Multidisciplinary efforts have been undertaken to develop economic analyses of transport system impacts that capture the underlying interdependencies between physical infrastructure and macroeconomic performance. Cho et al. [15] and Gordon et al.[16] link the transportation network model with the Input-Output (I/O) model by re-establishing interregional trade equilibria based on post-disaster changes in travel costs using a gravity model. They then estimate output changes from the updated I/O relationships and reduced final demands due to direct losses. Similarly, Sohn et al. [17] employ an I/O framework, but they derive production loss ratios from the transportation network resiliency of economic sectors and apply these ratios directly to modify sectoral outputs. Wei et al. [18] propose a combined supply- and demand-side I/O approach, where increased travel time and distance are translated into higher commuting costs. These cost increases are used to assess supply-side effects on consumer expenditures and, subsequently, total output losses from reduced final demand. Besides I/O-based methods, Koc et al. [19] and Wei et al. [20] develop the Comprehensive Resilience Assessment Framework for Transportation Systems in Urban Areas (CRAFT), which integrates a multi-regional Computable General Equilibrium (CGE) model, TERM, to analyze disruptions to both port and transportation networks. This framework captures reductions in port capacity and increases in transportation costs for freight delivery, allowing the model to re-establish equilibrium through adaptive agent optimization and to quantify the resulting macroeconomic impacts.

Many of these approaches center on the consequences related to travel costs, but the direct translation of generalized transport costs from network models into firms' actual transport expenses has been questioned by Tavasszy et al.[21]. They point out that generalized costs in transport models primarily reflect user preferences or travel efficiency, whereas actual transport costs are determined by market dynamics. In addition, there is significant uncertainty about the speed at which prices can adjust to restore economic equilibrium in the aftermath of disasters [22], an aspect rarely addressed in these models. Moreover, most of the work rely on macroeconomic models primarily used for static analysis, which overlook the dynamic

evolution of post-disaster conditions and interactions between physical and economic activities. Static models typically assume instantaneous adaptation and equilibrium restoration, failing to capture transitional disequilibrium [23].

Recent modeling advances have begun to incorporate dynamic frameworks. Colon et al. [1] assess the economic consequences of supply chain disruptions using an Adaptive Regional Input-Output (ARIO) model, where the indirect loss is computed as the sum of the increased final good price due to elevated travel costs and the consumption or production loss propagated from the input shortages. Brown et al. [24] use MERIT, a dynamic CGE-based model, to evaluate the economic impacts of inaccessibility through increased transportation costs, traffic redistribution, and relocation. Despite advances in capturing temporal changes during post-disaster recovery, both studies primarily focus on macroeconomic performance trajectories after disasters without explicitly examining the mechanisms through which inter-system interactions compound disruptions and hinder economic recovery.

To address the limited representation of physical infrastructure–economic interdependencies and the lack of modeling capability for identifying time-varying cross-system recovery bottlenecks, we develop a modeling framework that integrates transport system models with a macroeconomic model through a dynamic interface. Instead of linking the two systems through price mechanisms, the framework explicitly represents the physical interdependencies between transport and economic systems via their effects on labor and freight mobility. This physics-based integration enables the identification of how disruptions in individual infrastructure systems propagate through economic activities, revealing critical bottleneck periods and pinpointing where within the economic dynamics these constraints emerge. We apply the framework to evaluate transport system disruptions and their resulting economic impacts in the San Francisco Bay Area following a scenario earthquake.

The rest of the paper is organized in the following structure. We first provide an overview of the proposed modeling framework. Then we describe the case study context and detail the data and models used for the hazard and system impact analyses. Finally, we present the results and discuss their implications for multi-system resilience and potential mitigation strategies in the San Francisco Bay Area.

2. Integrated system modeling framework

To integrate the evolving physical infrastructure disruptions and economic system dynamics following a disaster, a typical modeling framework begins with simulating a disaster scenario using hazard-specific intensity measures, followed by damage and recovery analysis of the physical systems, and then evaluation of the resulting indirect economic impacts. In this study, we consider three key physical systems, buildings, road networks, and ports, and their downstream effects on regional economic activities. Thus, our modeling framework consists of five modules (Figure 1): (1) hazard simulation, damage and recovery analysis for (2) buildings, (3) road networks, and (4) ports, and (5) a dynamic macroeconomic model.

We propose a dynamic modeling interface to translate physical disruptions into time-varying economic shocks. Specifically, building damage is mapped to productive capital losses and reconstruction demand; road network disruptions constrain labor availability and mobility; and port damage leads to shocks in international trade, affecting import- and export-dependent sectors. We do not explicitly model the impacts of road network disruptions on goods movement, since freight traffic exhibits greater operational flexibility than commuter traffic, with freight operators able to adapt through rerouting, off-peak scheduling, and temporary overloading [25, 26]. These sector-specific shocks are fed into a dynamic macroeconomic model, which simulates the propagation of disruptions and the evolution of economic activity over time. As physical systems gradually restore their functionality after the disaster, the corresponding economic shocks evolve until both physical and economic systems are fully recovered.

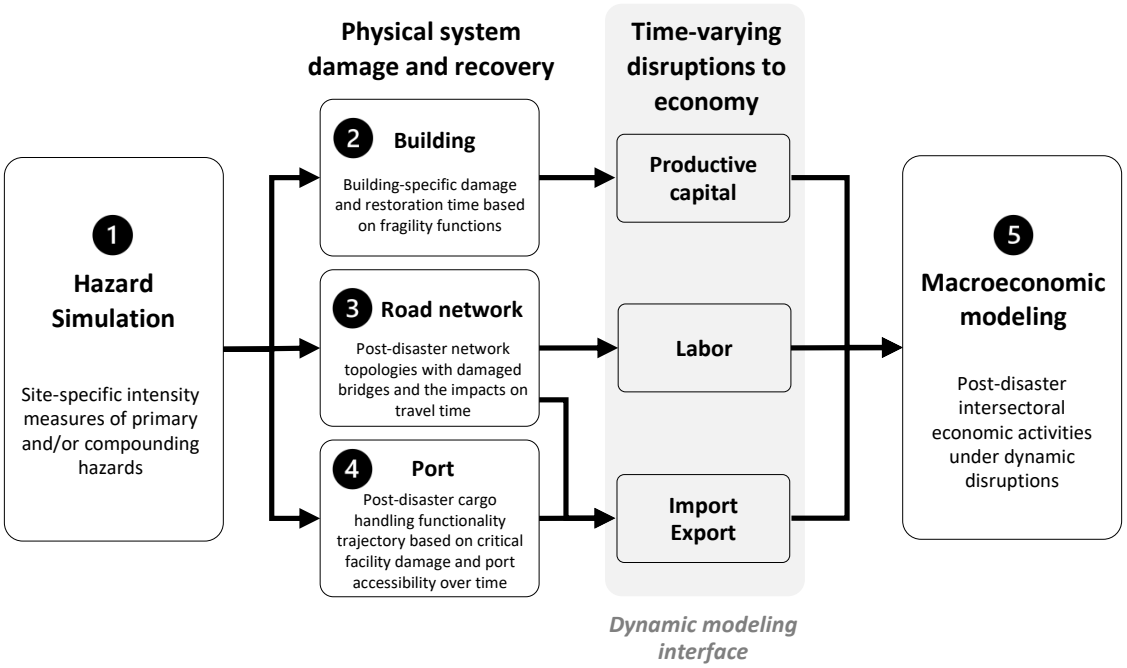


Fig. 1. Proposed framework for integrated system modeling.

Implementing this interface requires harmonization of spatial and industrial resolutions across models. Physical system analyses are often conducted at fine spatial scales, such as at the building level for structural damage or at the census block level for road network impacts, whereas economic impacts are evaluated at the regional level. To reconcile these discrepancies, we aggregate the estimated physical disruptions to represent regional economic shocks. Moreover, differentiation of shocks by economic sector is essential for economic analysis. This is achieved by obtaining and integrating information on building occupancy-industries mapping, the spatial distribution of employment by sector, and sector-specific freight and port operation data.

The hazard simulation module generates disaster loads for the specified hazard scenarios. For earthquakes, this includes spatially correlated ground motion intensity measures such as peak ground acceleration (PGA) and spectral accelerations (SA). We also account for permanent ground deformations (PGD) from induced hazards, such as landslides and liquefaction, which are particularly critical for infrastructure system vulnerability.

Using these site-specific intensity measures, we assess damage to buildings and transport systems. Building damage states are determined through fragility functions based on building type, from which repair costs and recovery times are estimated. The results are aggregated by economic sector to quantify sector-specific productive capital reductions, expressed as the ratio of repair costs to replacement values within each sector. This approach is consistent with previous applications of the Adaptive Regional Input-Output (ARIO) model [e.g., 27, 28]. While repair costs may not fully capture functional disruptions at the facility level, they provide a practical sector-level indicator of capital impairment in the absence of more detailed information on post-disaster production capacity. Meanwhile, damage generates additional demand for reconstruction, which is allocated to the sectors responsible for recovery activities, typically construction

and manufacturing sectors.

For the road network analysis module, we identify bridges as critical nodes for the network disruption, as bridge damage is the dominant source of prolonged road network disruptions in past California earthquakes and regional seismic risk assessments [29, 30, 31, 32]. Damage assessments yield the functionality loss and recovery timelines for bridges. To capture the consequences for labor mobility, peak-hour commuting trips are assigned to the disrupted road network at successive post-disaster periods to generate updated estimates of travel times. Adopting the cumulative opportunities measure for accessibility [33], a threshold on maximum tolerable commuting time is applied to determine labor accessibility constraints, and the resulting sectoral labor loss over time is computed based on the spatial distribution of the workforce.

In the port analysis module, we focus on the cranes and wharves as critical facilities governing port cargo handling capacity [34]. Damage assessments are first conducted at the component level and then aggregated to the system level to quantify time-varying reductions in cargo throughput. In this step, colocation effects are explicitly considered. Cranes located on a damaged wharf remain idle even if structurally intact, as berthing operations cannot proceed until the associated wharf is restored. Port functionality is further conditioned by accessibility. To capture this, we identify nearby highway bridges as critical nodes for port access and reduce the effective flow of goods into and out of the port in proportion to the traffic loss associated with disrupted connections.

Finally, we adapt the refined Adaptive Regional Input-Output (R-ARIO) model for macroeconomic modeling to enable dynamic integration with the physical system module outputs at discrete time steps during recovery. The R-ARIO is a dynamic model that simulates production and inter-sectoral interactions under disaster-induced shocks [35]. As an extension of the Input-Output models, R-ARIO not only captures demand-driven changes in output arising from disrupted inter-sectoral and household consumption, but also integrates supply-side constraints such as productive capacity losses, inventory depletion, and adaptive sectoral responses during recovery. The sector-level adaptive responses are characterized through behavioral parameters in the model, including maximum overproduction capacity, time to achieve maximum overproduction, target inventory level, time of inventory restoration, and heterogeneity parameter. The overproduction capacity represents the temporary capacity of sectors to produce above pre-disaster baseline levels during recovery. The heterogeneity parameter determines the extent to which inventory shortages constrain sectoral production. The model's dynamic structure provides a natural interface for incorporating time-varying shocks from the physical infrastructure modules as input model variables at different time steps. Through this integration, the R-ARIO model simulates how these evolving disruptions propagate across sectors and shape the trajectory of economic recovery. Moreover, the R-ARIO framework is adaptable and can be generalized to other study regions and hazard types by updating the underlying economic structure and shock inputs.

We introduce several modifications to the R-ARIO model to enable dynamic integration with the outputs of physical system modules. The R-ARIO model already distinguishes between imports and domestic production within the production calculation, where overproduction capacity is applied only to domestic production while imports are modeled independently. This formulation enables different external supply dependencies and disruption effects to be incorporated for the two components. In R-ARIO's original formulation, the productive capacity of sectors is modeled as a function of productive capital, which evolves with building damage and recovery. To incorporate additional constraints from labor, we extend the formulation to evaluate productive capacity as jointly determined by both capital and labor availability. Given the structure of the R-ARIO and its treatment of other model mechanisms, which do not allow for substitution between inputs, we adopt the Leontief production function. This specification assumes fixed input proportions and rules out substitution between labor and capital. While this formulation is consistent

with the fixed-coefficient structure underlying the ARIO framework, it does not capture potential adaptive responses through factor substitution. As a result, the estimated impacts of labor constraints may be higher than a specification allowing substitution between labor and capital. Relaxing this assumption, for example through a CES production function calibrated to empirically estimated capital-labor substitution elasticities, is a direction for future refinement of the model. We update the computation of the productive capacity accordingly as:

$$P_p^{cap}(t) = \alpha_p(t) \cdot \left(1 - \max\left(\frac{K_p(t)}{K_p^{pre}}, \frac{L_p(t)}{L_p^{pre}}\right)\right) \cdot P_p^{pre} + I_p(t) \tag{1}$$

where

$P_p^{cap}(t)$ = Production capacity of sector p at time t
$\alpha_p(t)$ = Overproduction capacity as the ratio to the pre-disaster production level of sector p at time t
$K_p(t)$ = Amount of damages to productive capital of sector p at time t due to building damage
K_p^{pre} = Pre-disaster fixed asset or productive capital of sector p
$L_p(t)$ = Amount of lost labor of sector p at time t due to road network disruption
L_p^{pre} = Pre-disaster workforce of sector p
P_p^{pre} = Pre-disaster production (excluding the imports) of sector p
$I_p(t)$ = Imports of sector p at time t

To incorporate the effects of port disruptions, we implement the export dynamics through an exogenous variable in sector demand computation at each time step:

$$D_p(t) = \sum_{all\ q} O_{q,p}(t) + C_p(t) + R_p(t) + E_p(t) \tag{2}$$

where

$D_p(t)$ = Demand to sector p at time t
$O_{q,p}(t)$ = Orders from sector q to sector p at time t
$C_p(t)$ = Total final demand to sector p at time t
$R_p(t)$ = Reconstruction demand to sector p at time t
$E_p(t)$ = Exports of sector p at time t updated based on port functionality and accessibility

We implement changing import as a factor in the production computation. Production is modeled as the sum of domestic output and imported inputs. After first computing the maximum possible domestic production, constrained by productive capacity and available inventories, the actual production of sector p at time t is determined as:

$$P_p^a(t) = min(D_p(t), P_p^{dom}(t) + I_p(t)) \tag{3}$$

where

$P_p^a(t)$ = Production of sector p at time t
$P_p^{dom}(t)$ = Maximum possible domestic production of sector p at time t

The details of how $P_p^{dom}(t)$ is computed are provided in Issa et al. [35] and the supplemental material. The supplemental material also provides more details on the model input, key parameters, and full model simulation process.

3. Simulation of San Francisco Bay Area earthquake scenario

We apply the framework to assess the indirect economic impacts of a magnitude 7.3 earthquake rupturing the Hayward fault in the San Francisco Bay Area, a region comprising nine counties. The Hayward–Rodgers Creek Fault system has an estimated 32% probability of producing a magnitude 6.7 or greater earthquake within the next 30 years [36]. We select the median-magnitude deterministic rupture scenario for the Hayward fault from the 2014 USGS National Seismic Hazard Maps [37]. In this analysis, we consider earthquake-induced damage to three critical physical systems: the building stock, the road network, and four major seaports that handle most of the region's foreign trade. These physical disruptions are dynamically integrated into a single-regional economic model to simulate the resulting indirect economic losses and recovery trajectories for 15 economic sectors classified by the U.S. Bureau of Economic Analysis (BEA) across the Bay Area. Although a deterministic hazard scenario is selected, we conduct Monte Carlo simulations with 1,000 realizations within each damage-analysis module to capture uncertainties in infrastructure damage and recovery times. The mean disruption and recovery trajectories of the physical systems are then used as inputs to assess the corresponding economic impacts.

3.1. Earthquake hazard

The disaster event analyzed in this case study is based on a magnitude 7.3 earthquake scenario developed by the U.S. Geological Survey (USGS). The scenario features an epicenter located at southeast Oakland and a depth of 8.8 km, with ruptures along the Hayward fault. Ground motion intensity measures, including peak ground acceleration (PGA), peak ground velocity (PGV), and spectral acceleration (SA) at a period of 1.0 second, are obtained at a spatial resolution of approximately 700 m across the Bay Area from the ShakeMap, which simulates shaking using empirical ground motion prediction equations (GMPEs) with site-response adjustments and spatial correlation [38].

In addition to direct ground shaking, we account for secondary ground-motion-induced hazards, specifically liquefaction and landslides, and their impacts on port infrastructure. We derive the permanent ground deformation (PGD) from PGA and PGV of the hazard scenario using SimCenter's Regional Resilience Determination (R2D) tool [39], which implements models from PEER's OpenSRA project [40]. The liquefaction model estimates both susceptibility and probability of occurrence and simulates lateral spreading and vertical settlement separately. The landslide model estimates earthquake-induced ground displacement based on local slope properties. For each site, the lateral PGD is computed as the sum of lateral spreading from liquefaction-induced and landsliding displacements, while the maximum of vertical and lateral PGD governs the overall damage caused by ground deformation. The compiled hazard intensity measures used in the analysis are shown in Figure 2.

3.2. Building damage and recovery

To conduct building analysis, we first generate a building-level inventory for the nine-county Bay Area using BRAILS (Building and Infrastructure Recognition using AI at Large-Scale) [41, 42], which fuses vector building footprints from OpenStreetMap (OSM) and the National Structure Inventory (NSI) with satellite and street-view imagery retrieved via the Google Maps API to infer or complete attributes needed for regional seismic risk analysis. We adopt BRAILS because it scales to region-wide coverage, yields a consistent schema that maps cleanly to HAZUS classes, and fills missing fields critical for fragility selection and economic aggregation.

We then simulate building-level damage and recovery time using a probabilistic damage and recovery modeling framework. For each building i, we use the Nearest Neighbor method to determine its associated intensity measures. Specifically identify its four nearest intensity stations and assign them with normalized

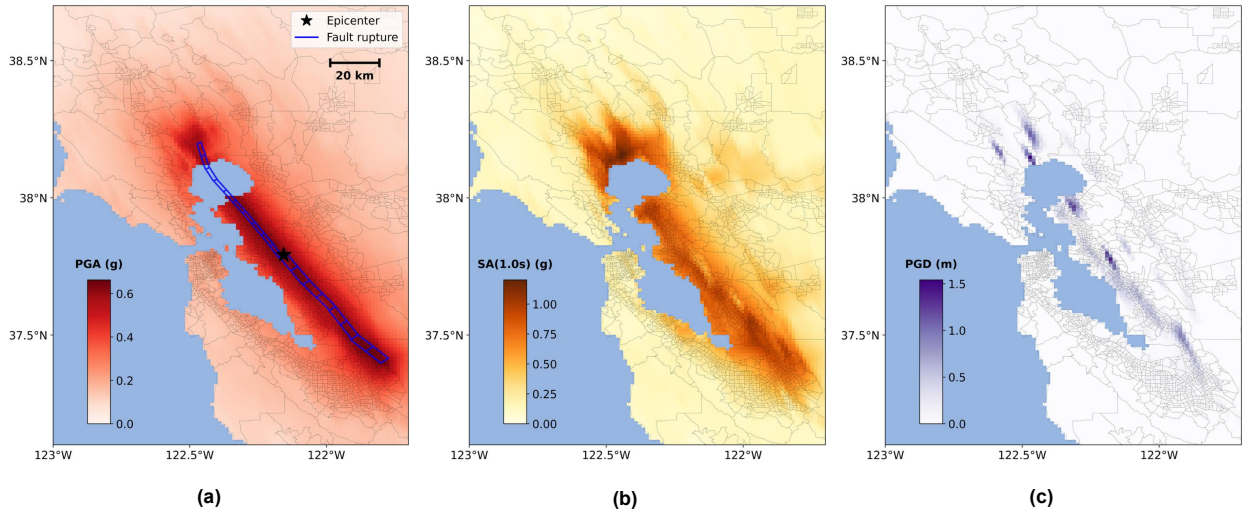


Fig. 2. Hazard intensity measures used in the analysis presented at the census tract level: (a) peak ground acceleration (PGA), and the surface projection of the fault rupture, (b) spectral acceleration (SA) at 1.0 second, and (c) permanent ground deformation (PGD) from liquefaction and landslides.

distance-decay weights. In each Monte Carlo realization r, one of the four stations is randomly selected with probabilities equal to these weights, and the building's PGA, $\text{PGA}_i^{(r)}$, is set to the selected station's PGA. This categorical draw preserves local heterogeneity while maintaining spatial coherence across buildings.

Given the sampled $\text{PGA}_i^{(r)}$ and building properties, we compute damage states using the HAZUS PGA-based fragility curves [43] through pelicun [44]. HAZUS also provides supplementary PGD-based damage relationships for shallow foundation settlement and lateral spreading. However, these relationships are based on engineering judgment and apply only to buildings with shallow foundations. Given that only 0.05% of buildings in this study are located in areas where HAZUS estimates a 0.5 probability of extensive or complete damage due to shallow foundation settlement and lateral spreading, we adopt the PGA-based fragility approach as a regional-scale simplification. HAZUS defines four damage states, *slight*, *moderate*, *extensive*, and *complete* damage, which corresponds to index $k = 1, 2, 3, 4$ respectively. The probability of exceeding for each damage state ds_k is computed as the standard normal cumulative distribution function of the natural logarithm of the ratio between $\text{PGA}_i^{(r)}$ and the median threshold θ_k, normalized by the logarithmic standard deviation β_k.

The probability of being in a specific damage state ds_k is then obtained by taking the difference between two consecutive exceedance probabilities:

$$\mathbb{P}\left\{\text{DS} = ds_k \mid \text{PGA}_i^{(r)}\right\} = \mathbb{P}\left\{\text{DS} \geq ds_k \mid \text{PGA}_i^{(r)}\right\} - \mathbb{P}\left\{\text{DS} \geq ds_{k+1} \mid \text{PGA}_i^{(r)}\right\}. \tag{4}$$

After obtaining the conditional probabilities of each damage state, a random number $u \sim \mathcal{U}(0, 1)$ is drawn for each building. The damage state is then assigned based on the interval in which u falls within the cumulative probability distribution.

State-dependent repair models map $\text{DS}_i^{(r)}$ to a repair-cost ratio $r_i^{(r)} \in [0, 1]$ (repair cost divided by replacement value) and a repair time $T_i^{(r)}$ to full functionality based on HAZUS. Here, repair-cost ratio and repair time are assigned deterministically conditional on damage state. The damage and recovery time simulation is implemented using SimCenter R2D application [41, 39] with DesignSafe [45] high-performance computing resources.

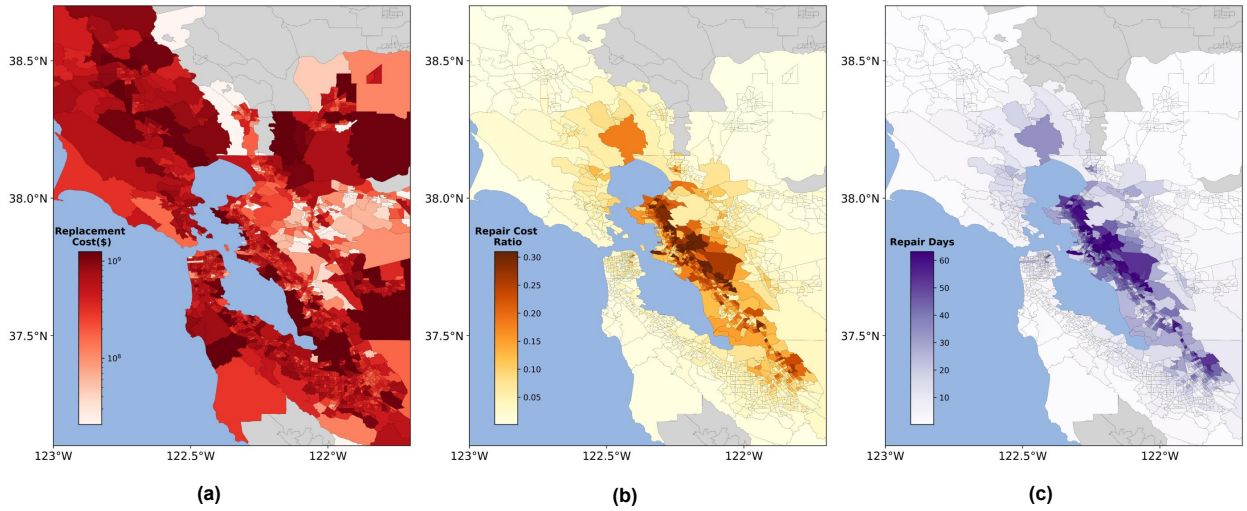


Fig. 3. Census-tract-level aggregated building recovery outcomes in the San Francisco Bay Area: (a) total replacement cost (USD); (b) mean repair cost ratio; (c) mean repair time averaged over buildings.

The tract-level summaries of building replacement values, repair costs ratio, and average repair time for Bay Area under the given earthquake scenario is shown in Figure 3. Over 1.5 million buildings we analyze for the study area, the total replacement value is $560 billion, and this earthquake results in a total mean repair cost of $48 billion.

We then categorize buildings into housing and 15 BEA economic sectors to derive sector-level trajectories of building asset value recovery following the earthquake. This categorization is based on the HAZUS occupancy-to-industry mapping scheme developed in the HayWired study [46]. In HayWired, HAZUS occupancy classes are mapped to the IMPLAN 46-industry classification. We further aggregate these industries into the 15 broader BEA sectors using established crosswalks between IMPLAN industries and NAICS classifications. The full mapping scheme is provided in the supplemental material.

In the HayWired mapping, a single HAZUS occupancy class may correspond to multiple IMPLAN industries. In these cases, we allocate each building's replacement value and simulated losses fractionally across the possible corresponding industries. For example, the HAZUS occupancy class *Industry 2* maps to four IMPLAN industries: *Oil and gas extraction*, *Coal mining*, *Other mining*, and *Primary metal manufacturing*. We therefore split *Industry 2* buildings' replacement values and repair costs evenly between these four industries, with each receiving a 0.25 share. These IMPLAN-level allocations are then aggregated to BEA sectors, resulting in three-quarters of the total value and losses assigned to the Mining sector (via *Oil and gas extraction*, *Coal mining* and *Other mining*) and the other one-fourth assigned to Manufacturing sector (via *Primary metal manufacturing*).

Under a threshold-type functionality assumption, each building is considered to regain full functionality at its repair time $T_i^{(r)}$. Before that point, the unrepaired loss remains constant, equal to the product of the building's replacement value and its repair cost ratio. Once t reaches or exceeds $T_i^{(r)}$, the loss instantly drops to zero, representing an abrupt recovery to full functionality. Then, the unrepaired loss of building i evolves as

$$L_i^{(r)}(t) = RV_i \, r_i^{(r)} \, \mathbf{1}\left(t < T_i^{(r)}\right), \tag{5}$$

where $L_i^{(r)}(t)$ denotes the unrepaired loss of building i at time t in realization r. RV_i is the replacement

value and the indicator function $\mathbf{1}(\cdot)$ takes the value 1 when the condition inside the parentheses is true and 0 otherwise.

At each time t, we compute sector-specific recovery rate by first summing the repair costs of the buildings that have not yet recovered (i.e., $T_i^{(r)} > t$), normalizing by the corresponding total replacement value to obtain the remaining loss ratio, and then taking 1 minus this ratio. Repeating this calculation over time traces a recovery trajectory.

Figure 4 shows the recovery trajectories of buildings by sector. The initial loss ratio of each sector represents the percentage of damaged productive capital immediately after the earthquake. The time-varying reconstruction rate $R^p(t)$ is determined as the slope of building recovery curve by sector, which is assigned as the dynamic reconstruction demand to the corresponding sectors in the economic model.

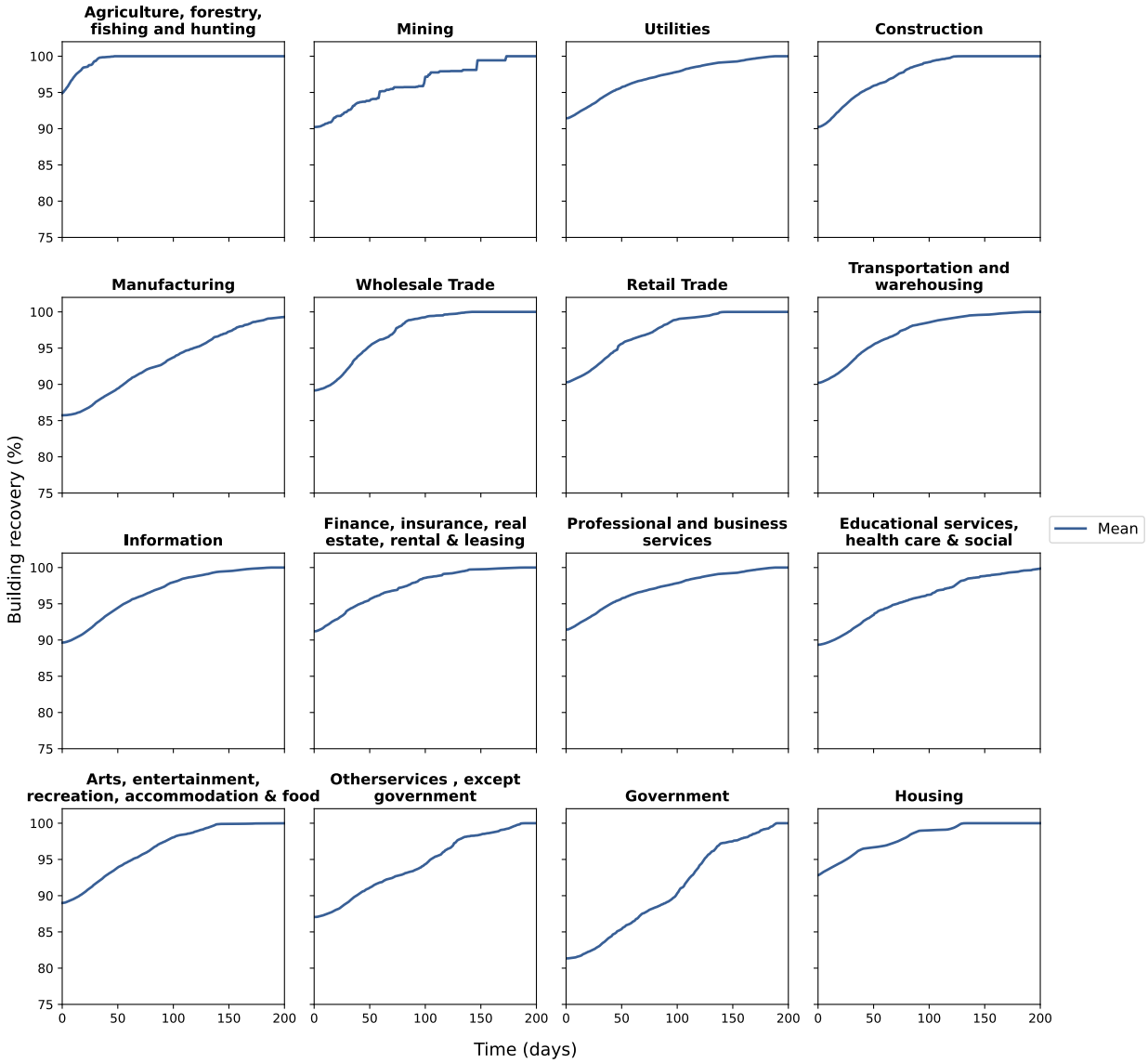


Fig. 4. Sectoral recovery trajectories following building damage in the San Francisco Bay Area. Each panel shows the time evolution of capital recovery for one of the 16 sectors (15 BEA sectors plus housing).

3.3. Road network disruption and recovery

The road network and flow model used in this study was developed by Miller [47]. The road network is represented through a graph of 11,921 nodes, connected by 32,588 edges, and includes 1743 bridges. The information on the bridges' fragility curves was provided by the Department of Transportation of California (Caltrans). To estimate travel times, we employ an iterative traffic assignment (ITA) algorithm that partitions total travel demand into four increments of 40%, 30%, 20%, and 10% of the total trips demanded [48]. This iterative algorithm assigns the first portion of 40% the trips using the shortest path between sets of origins and destinations, and then it updates the traffic along the traversed links according to their newly congested condition. The iterative traffic algorithm proceeds with the rest of the trips to assign in a similar fashion, computing the shortest path for each set of commuters in the updated congested state of the system.

We first simulate bridge damage states using bridge fragility functions developed by Caltrans based on site-specific SA at the period of 1.0 second. Consistent with HAZUS definitions, four damage states are considered. Bridges with damage states less severe than "extensive" are assumed to remain functional, while those classified as "extensive" or "complete" are rendered inoperable (Figure 5a). Recovery times are then assigned based on the bridge damage state. According to HAZUS, extensively damaged bridges require 75 days for repair, while completely damaged bridges require 230 days. Due to computational constraints, we do not incorporate uncertainty in bridge recovery times in this analysis. Accelerated bridge repair strategies have been implemented following some past disaster events; however, such measures are often highly targeted and depend on event-specific logistical and resource conditions [49, 50]. Therefore, accelerated bridge repair is not explicitly modeled in this study, but the corresponding impacts are expected to fall between the transportation-included and transportation-excluded recovery scenarios. Based on these recovery assumptions, we generate two representative road network graphs: (1) immediately after the earthquake, prior to the recovery of any extensively or completely damaged bridges, and (2) after extensively damaged bridges have recovered but before the recovery of completely damaged bridges.

We obtain the commuting demand in the Bay Area in 2021 at the census block level from the LEHD Origin-Destination Employment Statistics (LODES) database. For each origin–destination pair, the dataset provides total commuting flows across all sectors. These flows are assigned to the two disrupted road networks to simulate peak-hour travel times under the different recovery stages, assuming the commuting demand remains the same post-earthquake. We then apply thresholds of maximum tolerable commuting time, beyond which workers cannot reach their workplaces. Based on these thresholds, the number of workers unable to commute is calculated for each recovery stage (Figure 5b-c).

To translate lost trips into sector-specific labor impacts, we distribute the lost labor force proportionally to economic sectors based on the home census block's employment distribution across 20 detailed sectors. These sectors are then aggregated to the 15 broader sector categories in BEA classification to align with the economic analysis. Summing across all origins, we obtain the total number of workers lost per sector. The spatial distribution of employment is assumed to remain fixed throughout the analysis. This assumption is intended to represent the short-term recovery period, during which disruptions to labor accessibility are expected to dominate, whereas changes in employment relationships and sectoral labor reallocation typically occur over longer timescales than those considered in the present study [51, 52]. We further account for sector-specific remote-work adaptability by adjusting the estimated labor losses to exclude workers who are able to work remotely. Sector-level distributions of full-time telework workers in October 2022 from the U.S. Bureau of Labor Statistics [53] are used for this adjustment. We assume that remote-capable workers are uniformly distributed among employees regardless of whether they are able to commute after the disaster. Under this assumption, the lost labor ratio for each sector is reduced proportionally by the share of full-time remote workers, and the sector-specific percentage of labor unavailability is derived accordingly

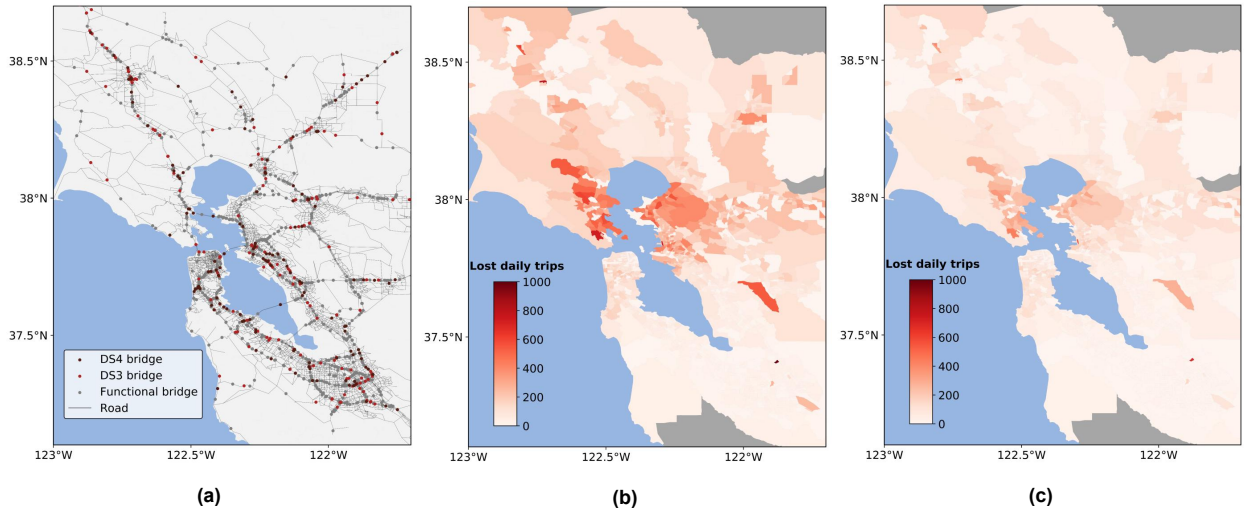


Fig. 5. (a) Road network in the Bay Area with median bridge damage status (DS4 = completely damaged and DS3 = extensively damaged) from simulation, (b) Spatial distribution of the mean daily lost commuting trips at the census tract level before extensively damaged bridges are repaired, and (c) Spatial distribution of the mean daily lost commuting trips at the census tract level after extensively damaged bridges are repaired but before completely damaged bridges are restored.

over time (Figure 6). Since driving and carpooling dominate commuting in the Bay Area [54], we do not consider alternative modes or post-disaster mode shifts in this analysis. Furthermore, the labor disruption estimates account only for commuting accessibility and do not explicitly consider other factors that may affect workforce availability, such as housing displacement, school closures, or disruptions to utilities and communication services. In addition, given California's relatively high seismic design standards, fatalities and injuries are not expected to impact a high percentage of individuals and households in the region. The HayWired study of a similar event in the same region predicted 800 deaths and 16,000 nonfatal injuries, which is 0.2% of the region's population of 8 million [55]. Given this small fraction, the labor force is not modified to reflect these impacts.

3.4. Port disruption and recovery

In this study, we consider four major seaports in the Bay Area: the Port of Oakland, the Port of Richmond, the Port of Redwood City, and the Port of San Francisco. Among these, the Ports of Oakland and Richmond handle the majority of the region's imports and exports, accounting for 39.7% and 51.9% of total freight tonnage in 2022, respectively [56]. Besides, the Bay Area also holds the Port of Benicia, a privately owned facility that specializes in commodities such as motor vehicles and bulk agricultural products. Due to limited data availability, this port is excluded from the analysis.

For each seaport, we compile the locations and geometries of cranes and wharves using port facility maps and manual digitization from satellite imagery. Structural damage for each component is assessed separately using PGA-based and PGD-based fragility functions from HAZUS. The damage state of the component is then determined as the more severe of the two assessments. Components reaching extensive or complete damage states are classified as non-functional. Each crane is assumed to contribute equally to port handling capacity. For wharves without cranes installed on the top, we segment them into vessel-sized lengths, with each segment assigned an equivalent functionality to a single crane. Recovery times for damaged components are sampled from state-dependent normal distributions provided in HAZUS (Table 1).

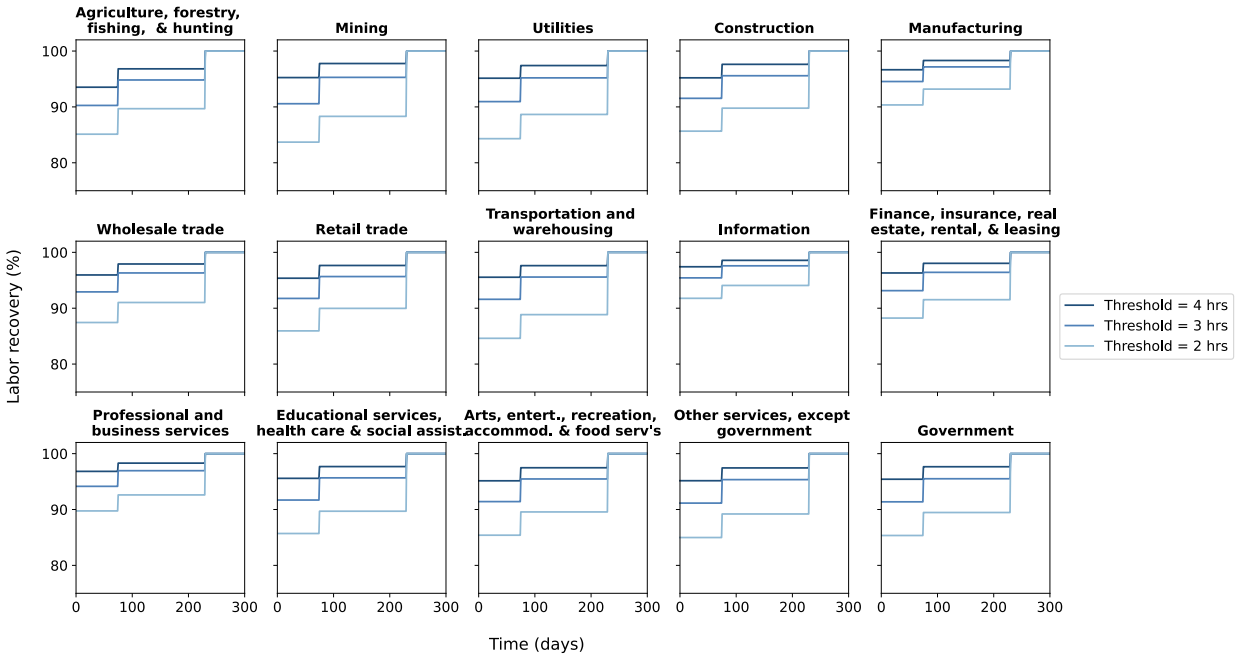


Fig. 6. Mean labor availability recovery trajectories by sectors based on road network damage and recovery under 4-hour, 3-hour, and 2-hour commuting time thresholds.

To account for port accessibility, we identify critical bridges that connect each port to the regional highway system from the satellite image. Using baseline truck traffic flows, we estimate the fraction of freight capacity lost when a given bridge is inoperable. Specifically, the reduction is calculated as the truck volume on the affected access link divided by the total truck traffic entering or exiting the port. The truck volume distributions at the normal day condition are obtained from Caltrans 2022 Truck Annual Average Daily Traffic (AADT). This procedure is applied to all ports using bridge damage realizations derived from the road network analysis. At each recovery stage, overall port functionality is defined as the minimum of (1) cargo-handling functionality from cranes and wharves and (2) truck accessibility from bridge connectivity (Figure 7).

To quantify sector-specific impacts, we use cargo handling statistics from port reports [56], which provide pre-disaster import and export distributions for agricultural, mining, and manufacturing products across ports (Figure 8). We assume that the percentage of affected cargo tonnage corresponds to the same percentage of affected import or export value for each sector. In the Bay Area, the Port of Oakland

Table 1. Normal distribution parameters for port component recovery times by damage state [43]. All values are in units of days.

Damage State	**Wharf**		**Crane**	
	Mean	Standard Deviation	Mean	Standard Deviation
Slight	0.6	0.2	0.4	0.35
Moderate	3.5	3.5	6	6
Extensive	22	22	30	30
Complete	85	73	75	55

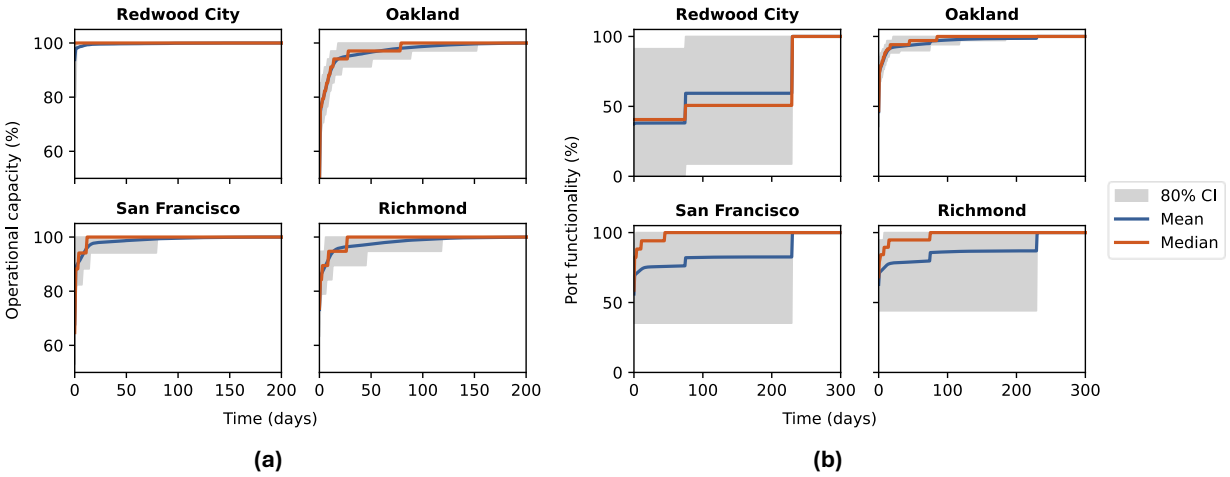


Fig. 7. Ports functionality trajectory after the earthquake (a) only considering cargo handling capacity from cranes and wharves, and (b) with additional constraints from truck accessibility from bridge connectivity. The grey area shows the 80% confidence interval across realizations.

dominates agricultural trade both into and out of the region and serves as the primary exporter for the mining sector. The Port of Richmond accounts for most of the imports and exports for the manufacturing sector. Meanwhile, the Port of Redwood City contributes significantly to mining imports. The ability of undamaged port facilities to temporarily increase throughput and accommodate rerouted trade flows from impaired ones is a common resilience mechanism in freight transportation systems during disruptions [57]. We further account for this excess operational capacity by applying a scaling factor of 1.1 to the remaining port functionality over time. This factor value is adopted from Wei et al. [20] and is consistent with the overproduction capacity for sectoral production in the R-ARIO model. Imports and exports for each sector are assumed to be flexibly redistributed among ports with available capacity within the Bay Area. Inter-regional rerouting to ports outside the region is not explicitly modeled in this study, as modeling such adaptation would require additional information on external port capacity, freight flows, transportation costs, and inland logistics constraints. This limitation may lead to conservative estimates of port-related disruptions. The time-dependent import/export flows for sector p are then calculated as:

$$I_p(t) = min\left(\sum_i I_{p,i}^{pre}, \sum_i I_{p,i}^{pre} \times F_i(t) \times \alpha^p\right), \qquad E_p(t) = min\left(\sum_i E_{p,i}^{pre}, \sum_i E_{p,i}^{pre} \times F_i(t) \times \alpha^p\right) \quad (6)$$

where

$$\begin{aligned} I_{p,i}^{pre} &= \text{Pre-disaster import of sector } p \text{ handled by port } i \text{ at a single time step} \\ E_{p,i}^{pre} &= \text{Pre-disaster export of sector } p \text{ handled by port } i \text{ at a single time step} \\ F_i(t) &= \text{Functionality of port } i \text{ at time } t \\ \alpha^p &= \text{Excess capacity factor of ports, assumed to be 1.1} \end{aligned}$$

Since import and export data are unavailable for other sectors beyond agriculture, mining, and manufacturing, we adopt two alternative assumptions to bracket the sectoral exposure to port disruptions: (a) only

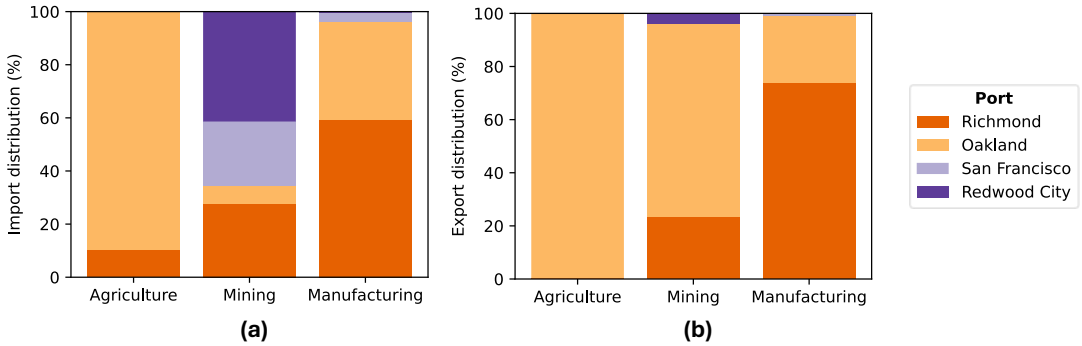


Fig. 8. Pre-disaster distribution of cargo tonnage handled by Bay Area ports for the agricultural, mining, and manufacturing sectors: (a) sectoral distribution of imports and (b) sectoral distribution of exports.

the agriculture, mining, and manufacturing sectors are directly affected by port disruptions (three-sector), and (b) other sectors experience disruptions equivalent to the average impact across these three sectors (all-sector). The three-sector assumption restricts the direct shock to the primary goods-producing sectors whose outputs and inputs transit through ports as physical merchandise, while the all-sector assumption distributes the shock across both goods-producing and services-producing sectors, providing an upper-bound scenario that accommodates unrecorded port dependencies. The resulting sector-specific import and export disruptions are illustrated in Figure 9.

3.5. Integrated economic disruption and recovery

We conduct a single-regional economic impact analysis for 15 sectors in the Bay Area, as defined by the BEA. The required input to set up the R-ARIO model for the study region includes the input–output (I-O) table, fixed asset values, and the sectoral behavioral parameters. The I-O table contains information on inter-sectoral trade, final demand, value added, exports, and imports. For this study, we derive the regional I-O table and fixed asset estimates for 2022 by applying the Regional Input-Output Modeling System (RIMS II) multipliers to the national BEA datasets, which construct the pre-disaster economic structure for the Bay Area. We adopt behavioral parameter values suggested in Issa et al. [35] for analysis based on the categories of sectors. These parameter values are derived from prior literature and empirical evidence on post-disaster business adaptation. A global variance-based sensitivity analysis of the behavioral parameters identified the target inventory level parameter for Manufacturing, Services, and Beverages+Food categories as the most influential on predicted indirect loss, while other behavioral parameters exhibited limited sensitivity [35].

In addition to these economic data, we integrate time-varying trajectories of sector-specific shocks, including asset loss and recovery, labor disruptions, and import/export constraints derived from the physical infrastructure modules. For each variable, the mean disruption and recovery trajectory from Monte Carlo simulations is used as input to the economic model. Therefore, the modeled indirect losses represent economic impacts associated with the mean physical disruption scenario, rather than the full probabilistic distribution of economic losses. This approach allows us to isolate the sensitivity of economic outcomes to key modeling assumptions, including travel behavior and the impacts of port disruptions on sectors, without conflating these effects with variability arising from the physical hazard and damage simulations. Together, these datasets constitute the complete input set for the R-ARIO simulation. The model is run over a three-year horizon following the earthquake, with economic dynamics simulated at a daily time step to capture the regional macroeconomic recovery process.

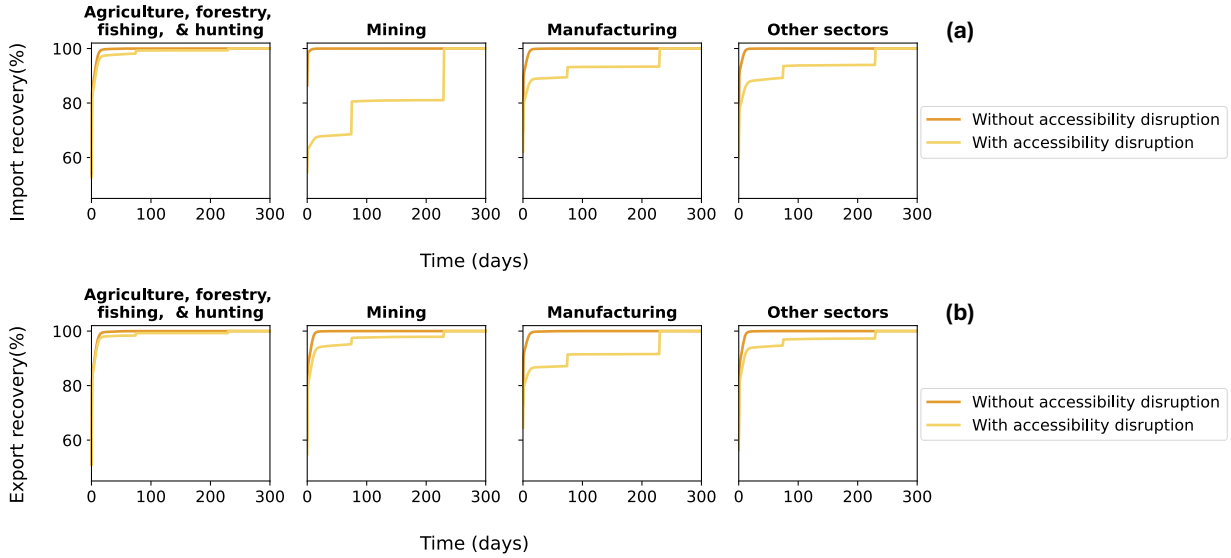


Fig. 9. Import (a) and export (b) recovery trajectories by sector, accounting for port cargo-handling capacity recovery with or without truck accessibility. Recovery curves for the agricultural, mining, and manufacturing sectors are derived directly from their pre-disaster trade distributions across ports, while recovery for all other sectors is approximated based on disruptions to overall port cargo handling.

This single-region analysis aggregates disruptions to the regional sector level and evaluates their impacts at the scale of the overall Bay Area macroeconomy. This approach captures the first-order regional consequences of coupled physical and economic disruptions. A multi-region extension of the R-ARIO model could further account for spatial heterogeneity in industrial structure, damage exposure, interregional trade, and recovery dynamics across subregions [58]. However, implementing such an extension would require substantially more detailed economic input data, including high-resolution interregional I-O tables and subregional sectoral statistics. Due to these data constraints, a multi-regional economic analysis is not conducted in the present study.

4. Modeling results and discussion

To quantify the role of transport-economic interdependency plays in the post-earthquake economic performance, we perform the regional indirect economic analysis using different variants of the model. We first run the R-ARIO model in its original form (building-damage-only model), which only considers the effect of building damage and recovery while keeping labor availability and foreign trade flows fixed at their pre-disaster levels. The transportation-disruption variant introduces labor constraints arising from the disrupted road network and reduced commuting accessibility, while the port-disruption variant incorporates dynamic changes in import and export capacity as port functionality recovers. The fully integrated variant combines both extensions, thereby accounting for the coupled effects of building, transportation, and port disruptions on regional production. Across all variants, we use value added as the primary performance metric to evaluate economic outcomes.

In the fully integrated variant, we select our baseline model with assumptions of a 3-hour maximum tolerable commuting time and that only agriculture, mining, and and manufacturing sectors are directly affected by port disruptions (three-sector assumption), subject to port accessibility constraints. There is no clear consensus on an appropriate baseline for commuting time thresholds. The definition of “extreme

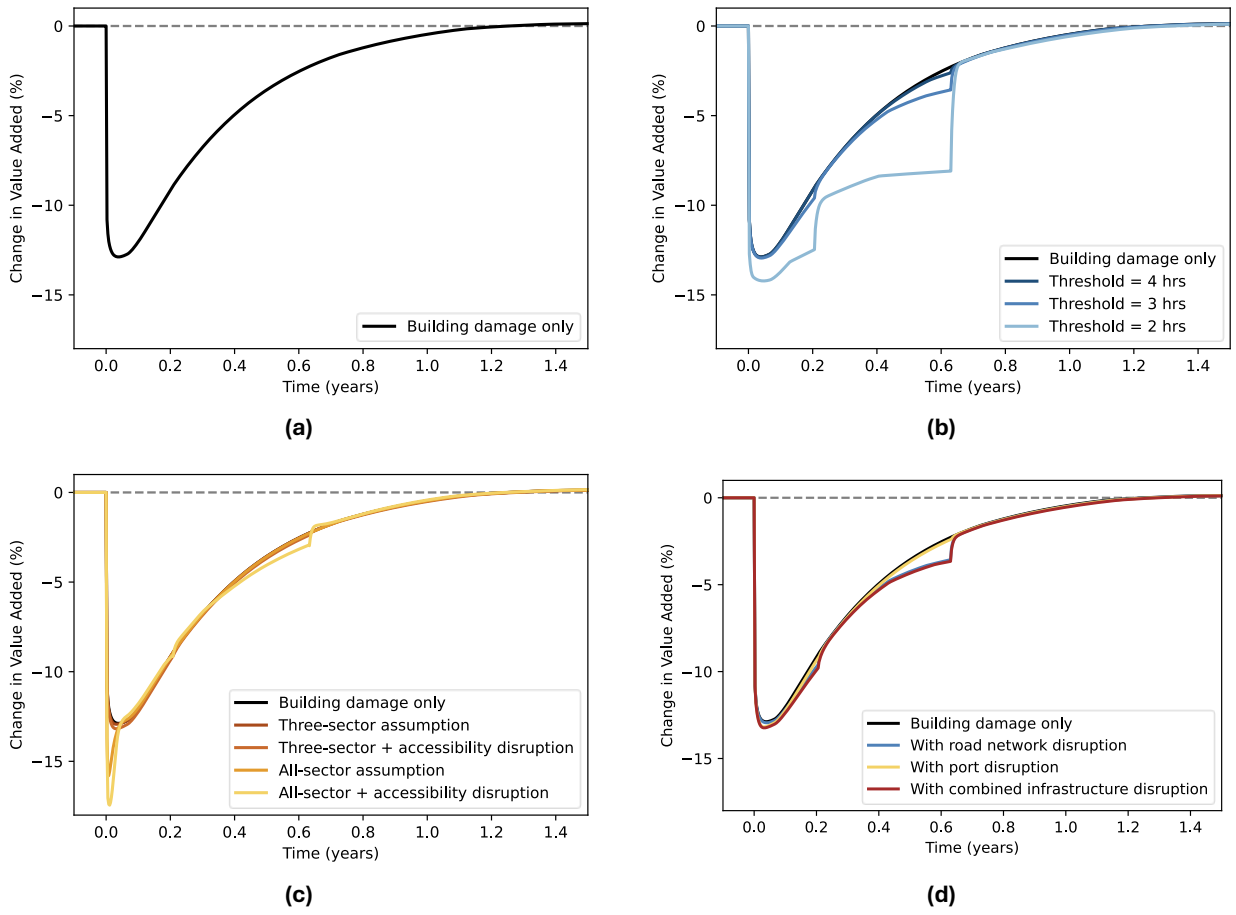


Fig. 10. Regional value added trajectory after the earthquake: (a) with original R-ARIO model considering building damage only, (b) R-ARIO model integrated with road network disruption, (c) R-ARIO model integrated with port disruption, and (d) R-ARIO model integrated with combined infrastructure disruptions (for baseline case).

commuters" implies that an extreme commuting time would exceed 90 minutes under normal conditions [59], while some post-disaster transportation impact studies use values as high as four hours [13]. We select a value of three hours to anchor the analysis while allowing alternative assumptions to bracket plausible upper and lower bounds. The three-sector assumption is adopted as the baseline because major port disruptions result in direct trade shocks to commodity flows that physically transit the seaports, with the agriculture, mining, and manufacturing sectors being the most affected. Given the uncertainties associated with travel behavior and the impacts of port disruptions on sectors, we also conduct a sensitivity analysis across various alternative modeling assumptions.

In this section, we first evaluate regional-level value added losses across model variants to quantify the total indirect economic impacts and cascading effects from disruptions to each infrastructure system in the Bay Area earthquake scenario. We then compare how these cascading impacts vary across individual sectors. Finally, leveraging the model's dynamic structure, we identify bottleneck periods during recovery when specific infrastructure disruptions constrain overall economic performance.

4.1. Regional economic impacts

With an estimated direct loss of $47.9 billion from building damages, the building-damage-only model projects an initial 12.9% drop in regional value added, followed by a recovery to pre-disaster levels within approximately 15 months (Figure 10a). The total cumulative loss in value added reaches $62.3 billion, equivalent to 4.92% of the region's pre-disaster annual output.

These results are broadly consistent with the USGS HayWired scenario where a slightly smaller earthquake of magnitude 7.0 rupturing the same Hayward fault is considered [55, 32]. Using HAZUS analysis, the HayWired study estimates $53 billion loss in building repair costs in the Bay Area, with the majority attributed to shaking damage from the main shock. It also performed an indirect economic impact analysis using a CGE model. That analysis estimated that the property damage and utility disruptions (including water, power, and communication) result in an indirect Gross State Product loss of $44.2 billion within six months following the earthquake, where the utility-induced indirect loss was estimated at less than $0.9 billion.

When incorporating labor constraints caused by road network disruptions, the total regional value added loss increases by approximately $0.3 billion, $3.3 billion, and $25.6 billion under maximum tolerable commuting time thresholds of 4, 3, and 2 hours, respectively (Figure 10b). Under the 4-hour and 3-hour thresholds, the regional economy experiences a similar initial drop in value added as in the building-damage-only case. However, additional loss in value added starts to accumulate towards the restoration times of damaged bridges (0.21 years for extensively damaged bridges and 0.63 years for completely damaged bridges). Significant improvements in value added are observed after these time points, as the recovery of bridge restores workforce mobility, which alleviates labor constraints across the regional economy. The step changes are more abrupt than would be seen in a real regional recovery, but we adopt them for consistency with the widely used Hazus model, and anticipate that a more continuous restoration would redistribute disruptions over time but lead to similar overall indirect losses. This pattern indicates that, at certain stages of the recovery process, productive capital restoration outpaces transportation infrastructure repair and makes mobility constraint a bottleneck for economic recovery. Under the most conservative assumption with a 2-hour commuting threshold, labor shortages become severe, driving both a deeper initial decline and a prolonged suppression of economic activity until full transportation recovery is achieved. The comparison across commuting time thresholds highlights that the cascading effects of transportation disruptions on the economy are highly sensitive to assumptions about commuter travel behavior and tolerance for extended travel times.

When incorporating port disruptions in addition to the building damage considerations, the regional value added loss also increases from the building-damage-only case (Figure 10c). Without accounting for accessibility constraints, the additional losses amount to $0.06 billion and $1.0 billion for three-sector and all-sector assumptions, respectively. When both port operational disruptions and accessibility limitations are considered, the additional losses rise to $0.8 billion and $2.5 billion, respectively. In contrast to the effects of labor disruptions, reductions in imports and exports can lead to a sharper initial decline in value added immediately following the earthquake, with most of the incremental losses occurring during the early recovery phase. The accessibility restriction can further cause additional bottleneck for economic performance throughout the bridge restoration period. The range of estimated port-related impacts across alternative assumptions reflects uncertainties in sectoral dependence on port activities and post-disaster freight adaptation, including the extent of rerouting and available excess operational capacity.

When both types of infrastructure disruptions are considered, the additional regional value added loss is estimated at $3.3 billion for the baseline case, while it ranges between $0.5 billion to $26.8 billion with different combinations of alternative modeling assumptions. Figure 10d illustrates the baseline case results.

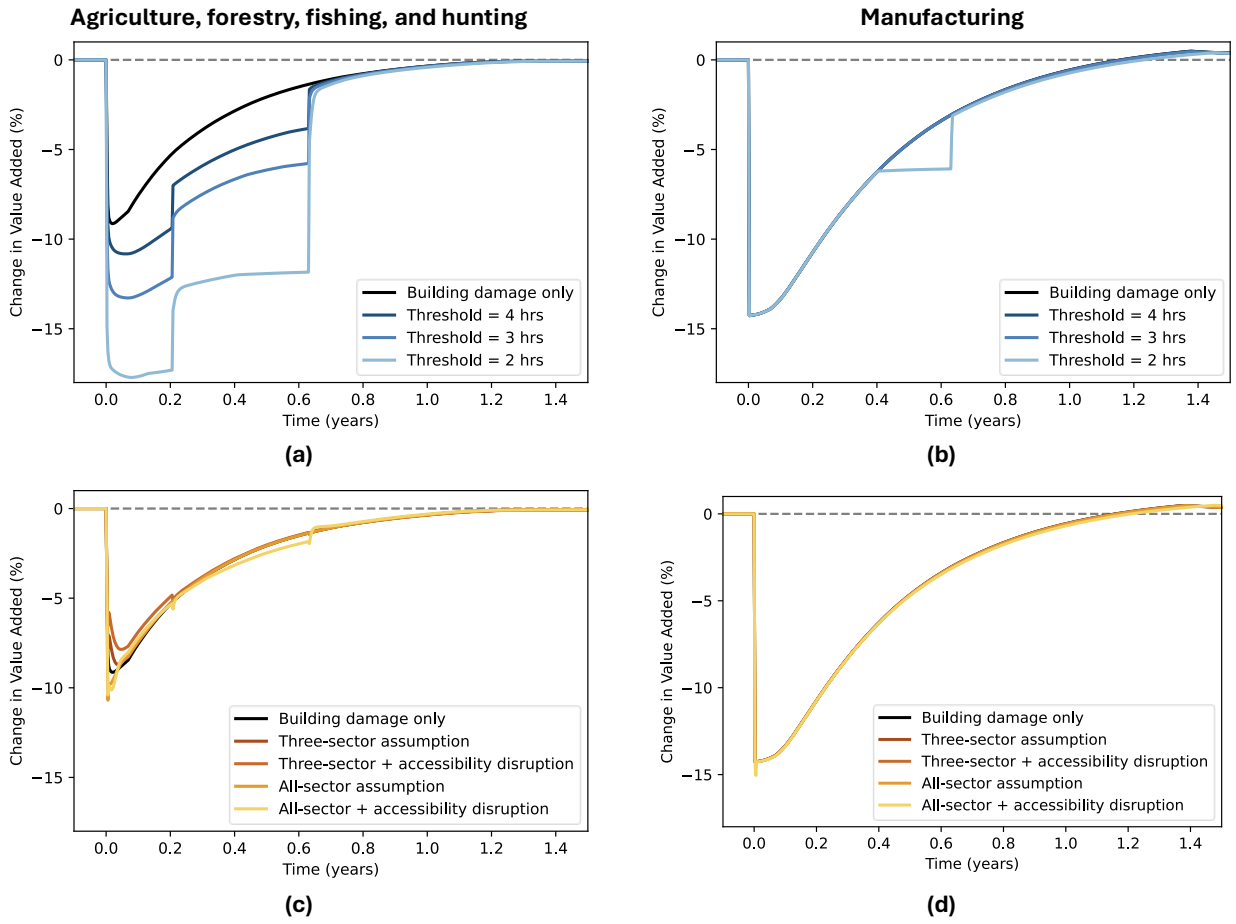


Fig. 11. Sectoral value added trajectory after the earthquake: R-ARIO model integrated with road network disruption (a and b) and R-ARIO model integrated with port disruption (c and d) for the agricultural and manufacturing sectors, respectively.

When only one type of infrastructure disruption dominates the building-damage-only model value added trajectory, the combined effect closely follows the same level of impact, as observed immediately after the earthquake. However, when both disruptions become critical relative to the building-damage-only model, their combined effect leads to greater losses than either disruption alone, though still smaller than the sum of their individual additional losses.

4.2. Sector-level economic impacts

We further evaluate sector-level economic performance across different model variants and find that the impacts of infrastructure disruptions vary substantially among sectors. The agriculture sector is the most sensitive to labor constraints induced by road network disruptions, with additional value-added losses ranging from 1.54% to 6.10% of its pre-earthquake annual value added (Figure 11a). The manufacturing sector is the least affected under the same conditions, with additional losses between 0.001% and 0.43% of its pre-earthquake annual value added (Figure 11b). This disparity arises from multiple factors. The manufacturing sector experiences more severe physical damage, which dominates its production capacity losses. Furthermore, the spatial distribution of workers, their commuting patterns, and the vulnerability of transportation links result in relatively lower mobility constraints for manufacturing labor than for the

agricultural sector in the Bay Area. Note that the agriculture and manufacturing sectors are largely ineligible for telecommuting. Thus, their labor supply is highly dependent on physical commuting conditions.

Port disruptions have divergent effects on sectoral value added. For the agricultural sector, although the combined impacts still result in an overall loss, port disruptions generate a positive effect on the sector's value added on top of the building-damage-only model value added loss under three-sector assumptions, with gains ranging from 0.05% to 0.20% of its pre-earthquake annual value added (Figure 11c). This outcome arises because, while export reductions lower external demand and thus production, simultaneous import reductions create opportunities for domestic substitution, which stimulates local production where capital constraints do not bind. This increase in value added reflects a redistribution from imports to domestic production within the model rather than an overall economic gain. Although value added increases relative to the building-damage-only case, total product availability remains lower because the reduction in imports is only partially offset by additional domestic production.

In contrast, the manufacturing sector experiences additional losses in value added from port disruptions, ranging from 0.002% to 0.07% of its pre-earthquake annual value added (Figure 11d). Beyond the decline caused by reduced exports, the import reductions have negligible offsetting effects on manufacturing output. This limited response may be due to this sector already operating near its domestic production capacity, driven by heightened reconstruction demand following the earthquake.

A full set of sector-level value added change results for all sectors is provided in the supplemental material.

4.3. Identifying vulnerabilities over time

Lastly, we investigate the bottlenecks in economic activities caused by the infrastructure disruptions and their temporal variations. Here, we focus our discussion on the baseline model case, though the same approach can be applied to other modeling assumption cases. In labor-intensive industries, bottlenecks emerge when productive capacity is constrained by labor input, i.e., when labor input is less than productive capital. Figure 12a shows the productive capacity loss by sector over time, with gray-bordered boxes marking periods when labor shortages govern the productive capacity. The duration and timing of these constraint periods vary by sector. In this case, agriculture and utilities sectors experience the longest labor-driven constraints, whereas manufacturing and government sectors show no such limiting effect throughout the recovery. The heterogeneity in bottleneck effects across sectors can be attributed to several factors. First, labor availability is affected differently across sectors due to variations in commuting patterns and remote-work adaptability. Second, the relative importance of labor constraints compared to productive capital constraints differs by sector. In some sectors, severe productive capital losses caused by building damage dominate production and partially mask the impacts of labor shortages. In contrast, although the finance sector has relatively high remote-work adaptability, it also experiences relatively small productive capital losses. Consequently, labor availability remains the dominant production constraint in this sector despite its comparatively low absolute labor losses. Most sectors face labor-related constraints around 75 days and again between 150–230 days post-earthquake. These periods correlate to the restoration timelines of bridges with different damage states. This finding suggests that the indirect economic impacts from the road network disruption can be potentially minimized if the restoration of critical transportation nodes is expedited.

Port disruptions influence economic activity through two primary mechanisms. The first is the reduction in exports, which lowers external demand and can directly constrain sectoral production. To identify when this export-related demand constraint becomes critical, we plot the trajectory of sectoral demand relative to pre-earthquake levels, highlighting periods when reduced exports govern production (Figure 12b). The agriculture sector experiences export-driven bottlenecks throughout the period of recovery of port facilities and accessibility in this case. In contrast, the manufacturing sector does not experience an export-driven

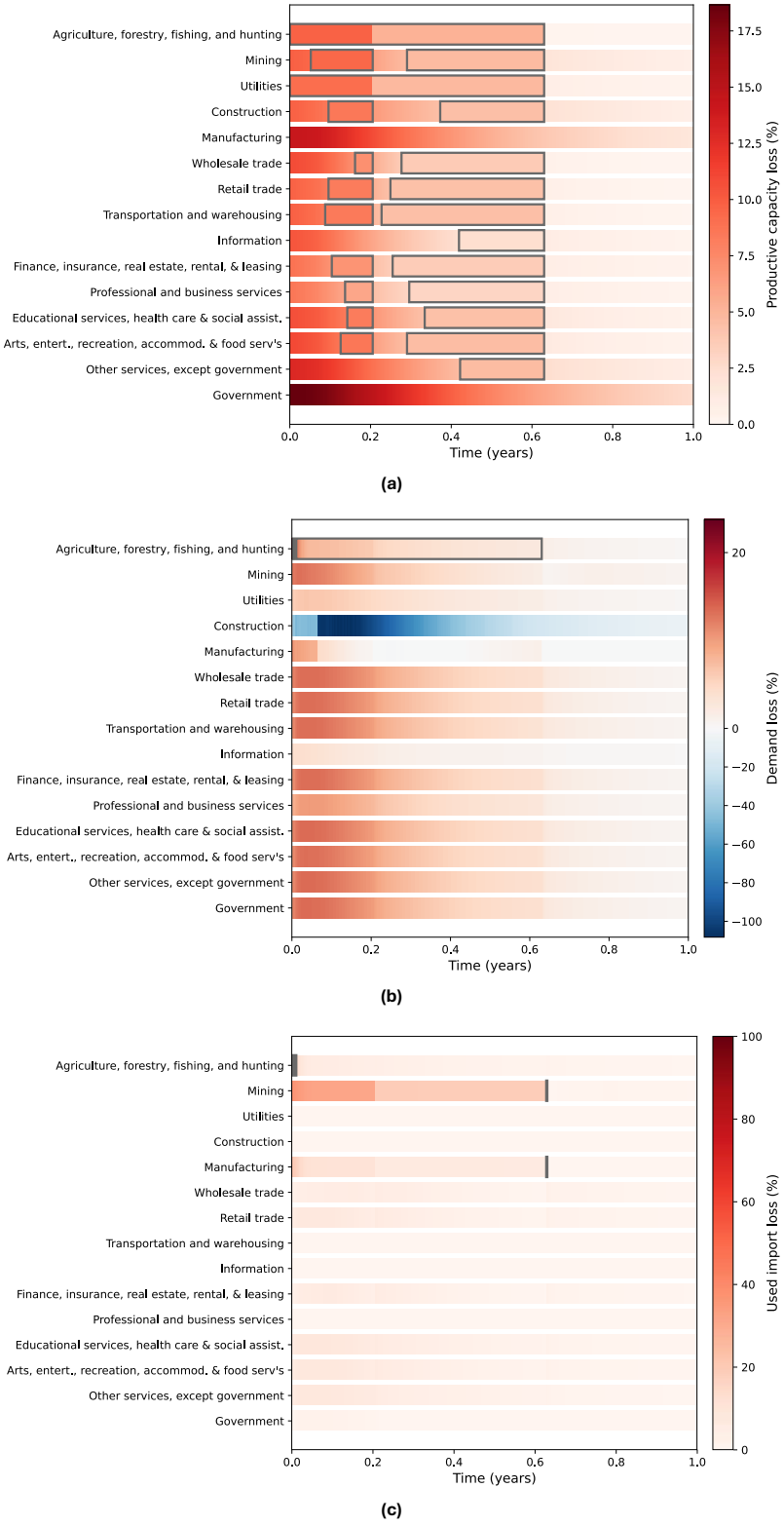


Fig. 12. Sectoral trajectories of (a) productive capacity, (b) demand, and (c) used import losses following the earthquake. Gray boxes indicate periods when (a) labor shortages, (b) reduced exports, and (c) reduced imports govern sectoral production, respectively.

production constraint because additional demand for reconstruction offsets the reduction in exports, while in the mining sector, productive capacity remains lower than reduced demand, thereby continuing to constrain output. These findings suggest that mitigating the scale or duration of port disruptions, utilizing alternative transport modes such as air or land routes, or stimulating substitute domestic demand, could reduce the indirect economic losses associated with disrupted exports.

The effects of import reductions stemming from the port disruption on economic performance are less straightforward to evaluate, as the import change does not directly affect the value added associated with domestic production. We instead focus on its effect on the overall sectoral production, which shapes supply chain performance and the recovery of productive capital. The metric we select to capture this effect is the used import in the production (Figure 12c). When demand is low, not all imports are required, and reductions in import availability may not be binding. Critical periods occur when sectoral demand exceeds production capacity, and uninterrupted imports could have alleviated the constraints on production. In this case, import-related bottlenecks last only a few days immediately after the earthquake and again toward the end of the port accessibility recovery period for most sectors. Although these bottlenecks are relatively short-lived, sourcing supplementary imports through alternative routes during these periods or minimizing port downtime could still enhance overall regional economic recovery.

Overall, the periods identified for each sector under different infrastructure disruption effects highlight both the vulnerabilities embedded within the transport–economy system and the opportunities for targeted intervention. These sector- and time-specific bottlenecks reveal when and where disruptions to transportation and port systems most strongly constrain economic recovery, offering actionable insights for prioritizing the restoration of critical transport facilities and optimizing resource allocation to shorten or eliminate these constrained periods and/or reduce the scale of disruption during bottleneck phases.

5. Conclusion

In this study, we developed a dynamic modeling framework that integrates transport infrastructure system damage and recovery into regional economic impact assessment. The framework adopts a modular structure comprising hazard simulation, physical system damage and recovery modeling, and an adapted Refined Adaptive Regional Input–Output (R-ARIO) model for macroeconomic recovery simulation. The analysis accounts for three key physical systems, including buildings, road networks, and ports, and their disruptions are translated into economic shocks through changes in productive capital, reconstruction demand, labor availability, and import–export dynamics, respectively. By dynamically linking the evolving physical system states with the economic model inputs, the framework captures the temporal evolution of interdependencies between physical and economic systems after disasters. This integrated approach enables investigation of both magnitude and temporal characteristics of cascading impact on economic performance from different infrastructure systems, both at the regional level and for specific economic sectors.

We applied the framework to assess the indirect economic impacts in the San Francisco Bay Area after a magnitude 7.3 earthquake at the Hayward fault. The physical system modeling estimates a direct loss of $47.9 billion from building damages. In the economic analysis that accounts only for building impacts, the region experiences an indirect loss in value added of $ 62.3 billion. When incorporating road network and port disruptions, the additional indirect losses is estimated at $3.3 billion with modeling assumptions of a 3-hour maximum tolerable commuting time and that only agriculture, mining, and and manufacturing sectors are directly affected by port disruptions subject to port accessibility constraints. We found that the two infrastructure systems exhibit distinct influences on the loss trajectory. Road network disruptions cause more pronounced losses towards the end of bridge recovery, while port disruptions lead to a sharper decline in value added immediately following the earthquake.

Different sectors show varying sensitivities to the two types of infrastructure disruptions. The agricultural sector is more vulnerable to transportation and port disruptions than the manufacturing sector in the Bay Area. This difference can be attributed to the relative extent of building damage, the spatial distribution of workers, their commuting dependencies on critical bridges, and the sector's reliance on imports and exports. Interestingly, port disruptions can have contrasting effects on sectoral value added. While reduced exports lead to additional losses, import reductions can, in some cases, stimulate domestic production to meet unmet demand, resulting in a temporary boost in value added.

We further investigated key economic metrics that capture the bottlenecks introduced by infrastructure disruptions during recovery. We identified that labor shortages, export reductions, and import constraints directly limit productive capacity, demand, and the use of imports in production, respectively. For each of these constraints, we determined the periods when their effects govern sectoral economic performance. In this case, most bottlenecks occur immediately after the earthquake and right before the recovery of bridges and port functionality. These findings suggest that accelerating the restoration of physical systems or implementing targeted mitigation strategies, such as sourcing substitute domestic demand or alternative inputs during critical periods, can effectively reduce cascading economic losses from infrastructure disruptions.

Overall, this analysis advances understanding of cascading economic losses arising from physical–economic system interdependencies and reveals the temporal dynamics of these impacts. The sensitivity analysis demonstrates that the uncertainties associated with the commute time threshold and commodities flow information can lead to substantially different estimates of economic impact. While opportunities remain to reduce these modeling uncertainties, such as through detailed assessment of post-disaster travel behavior or adaptive port operation analyses, the modular design of the framework provides flexibility to integrate advanced models as they become available. The framework can also be applied to other geographic contexts beyond the Bay Area with adaptation of model inputs and transportation components to reflect local economic structures and transportation dependence conditions. The modeling results offer actionable insights for resilience planners by pinpointing sector-specific bottlenecks and associated critical periods, enabling targeted strategies to mitigate these impacts.

6. Acknowledgements

The authors thank Jingyan Zhao and Adam Zsarnoczay from the SimCenter for their technical support and guidance in the use of the R2D tool, which facilitated the analyses conducted in this study. This work was supported in part by the National Science Foundation under NSF grant number CMMI-2053014. Any opinions, findings, and conclusions or recommendations expressed in this material are those of the authors and do not necessarily reflect the views of the National Science Foundation.

7. Supporting Information

Code implementing the adapted Refined Adaptive Regional Input-Output (R-ARIO) model is available at: https://github.com/tingerzhu/transport-R-ARIO.

8. Supplemental material

8.1. Refined Adaptive Regional Input-Output (R-ARIO) model for economic modeling

In this section, we describe how the adapted R-ARIO model is used to simulate post-disaster economic recovery. Table 2 lists the notations used in the model formulation, and Table 3 summarizes the sector-specific behavioral parameter values adopted in the analysis.

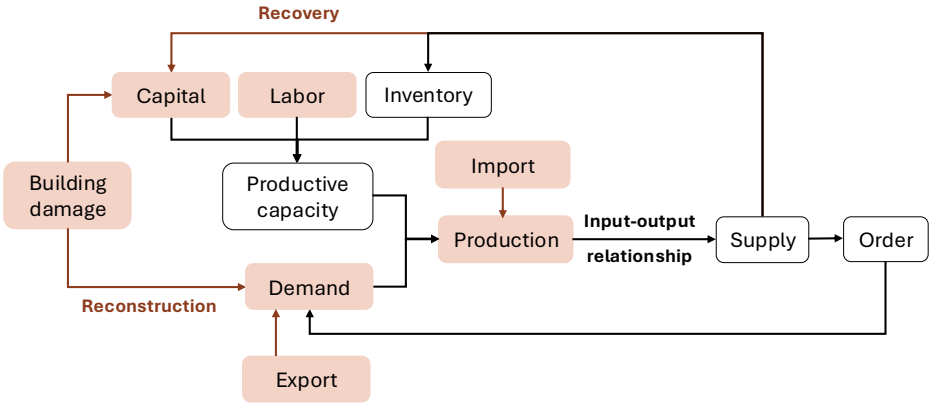


Fig. 13. Overview of the sectoral simulation process in the R-ARIO model at each time step. Red boxes indicate disaster-induced shocks considered in the model. Labor availability inputs are derived from the road network disruption analysis, while changes in import and export inputs are obtained from the port analysis.

The model simulates post-disaster economic activity at discrete time steps. Figure 13 provides an overview of the sectoral processes modeled at each time step. Sectoral output is jointly determined by production capacity and demand. The production capacity of each sector depends on the availability of productive capital, labor, and inventory. Based on realized production, goods and services are allocated proportionally between intermediate sectoral demand and final consumer demand. As reconstruction demands are progressively fulfilled over time, the productive capital stock of damaged sectors recovers accordingly. At the end of each time step, unsatisfied demand and sectoral orders are updated for the following step, and the value added generated by each sector is computed and tracked throughout the recovery process. The detailed model computations are described below.

First, demand $D_p(t)$ for each sector p at time step t is computed as the sum of intermediate orders, total final demand, reconstruction demand due to damaged productive capital, and exports:

$$D_p(t) = \sum_{\text{all}q} O_{q,p}(t) + C_p(t) + R_p(t) + E_p(t) \tag{7}$$

The demand can be satisfied by production in sector p, which comprises both domestically produced commodities and imports. The production is first constrained by production capacity, $P_p^{cap}(t)$, determined by the available productive capital and labor:

$$P_p^{cap}(t) = \alpha_p(t) \cdot \left(1 - \max\left(\frac{K_p(t)}{K_p^{pre}}, \frac{L_p(t)}{L_p^{pre}}\right)\right) \cdot P_p^{pre} + I_p(t) \tag{8}$$

The actual production, $P_i^a(t)$, is further constrained by available inventory at time t. To account for the effect from inventory, we first compute sector p's required inventory levels $S_{q,p}^r(t)$, which represents the amount of input q necessary to meet the local production level of sector p over the duration of inventory q:

$$S_{q,p}^r(t) = \begin{cases} \eta_q \times \left(P_p^{cap}(t) - I_p(t)\right) \times A_{q,p} & \text{if } D_p(t) > P_p^{cap}(t) \\ \eta_q \times D_p(t) \times \dfrac{P_p^{cap}(t) - I_p(t)}{P_p^{cap}(t)} \times A_{q,p} & \text{if } D_p(t) \leq P_p^{cap}(t) \end{cases} \tag{9}$$

The maximum possible production of sector p, $P^{max}_{q,p}(t)$, depends upon the actual inventory level of input q. If the required inventory $S^{r}_{q,p}(t)$ is not met, then the maximum possible production is reduced proportionally, taking into consideration inventory substitution effects (heterogeneity):

$$P^{max}_{q,p}(t) = \begin{cases} \left(P^{cap}_{p}(t) - I_p(t)\right) \times \min\left(1, \dfrac{S_{q,p}(t)}{\psi_q \times S_{q,p}(t)}\right) + I_p(t) & \text{if } D_p(t) > P^{cap}_{p}(t) \\ \min\left(D_p(t), D_p(t) \times \dfrac{P^{cap}_{p}(t) - I_p(t)}{P^{cap}_{p}(t)} \times \min\left(1, \dfrac{S_{q,p}(t)}{\psi_q \times S_{q,p}(t)}\right) + I_p(t)\right) & \text{if } D_p(t) \leq P^{cap}_{p}(t) \end{cases} \tag{10}$$

The actual production $P^{a}_{p}(t)$ is then taken as the minimum of all sectoral constraints:

$$P^{a}_{p}(t) = \min\left(P^{max}_{q,p}(t), \text{for all } q\right) \tag{11}$$

When demand is not fully met by the actual production, the production is distributed proportionally to partially meet the intermediate orders, total final demand, reconstruction demand, and exports. The order for the next time step from sector q to sector p, $O_{q,p}(t + \Delta t)$, is then updated based on the current status:

$$O_{q,p}(t + \Delta t) = A_{p,q} \cdot P^{a}_{q}(t) + \frac{\Delta t}{\tau^{s}_{p}} \cdot (S^{t}_{p,q} - S_{p,q}(t)) \tag{12}$$

The overproduction capacity of sector p for the next time step is updated based on the sector adaptability and current insufficiency in production:

$$\alpha_p(t + \Delta t) = \alpha_p(t) + (\alpha^{max}_{p} - \alpha_p(t)) \times \frac{D_p(t) - P^{a}_{p}(t)}{D_p(t)} \times \frac{\Delta t}{\tau^{\alpha}_{p}} \tag{13}$$

Finally, the value added for sector p at each time step t, $VA_p(t)$, is computed and recorded as:

$$VA_p(t) = P^{a}_{p}(t) - I_p(t) - \sum_{all\ q} A_{q,p} \times P^{a}_{p}(t) \tag{14}$$

Table 2. Refined Adaptive Regional Input-Output (R-ARIO) model nomenclature.

Definition	Type	Description
$A_{q,p}$	Input	Input-Output table coefficients (required units of input from sector q to produce unit of sector p).
$C_p(t)$	Input	Total final demand to sector p at time t, derived from Input-Output table.
$D_p(t)$	Variable	Demand to sector p at time t.
$E_p(t)$	Input	Exports of sector p at time t from port analysis output.
$I_p(t)$	Input	Imports of sector p at time t from port analysis output.
K^{pre}_{p}	Parameter	Pre-disaster fixed asset or productive capital of sector p.
$K_p(t)$	Variable	Amount of damages to productive capital of sector p at time t, where $\frac{K_p(0)}{K^{pre}_{p}}$ is derived from building damage output.

Continued on next page.

Table 2 – continued from previous page.

Definition	Type	Description
L_p^{pre}	Parameter	Pre-disaster workforce of sector p.
$L_p(t)$	Variable	Amount of lost labor of sector p at time t, derived from road network disruption analysis output.
$O_{q,p}(t)$	Variable	Orders from sector q to sector p at time t.
$P_p^a(t)$	Variable	Actual production of sector p at time t.
$P_p^{cap}(t)$	Variable	Production capacity of sector p at time t.
$P_{q,p}^{max}(t)$	Variable	Maximum possible production of sector p.
P_p^{pre}	Input	Pre-disaster production (excluding the imports) of sector p, derived from Input-Output table.
$R_p(t)$	Input	Reconstruction demand to sector p at time t, derived from damaged building recovery rate by sector.
$S_{q,p}(t)$	Variable	Actual inventory of input q for sector p at time t.
$S_{q,p}^r(t)$	Variable	Required inventory of input q for sector p at time t.
$S_{p,q}^t$	Parameter	Target inventory level of input q for sector p.
$VA_p(t)$	Variable	Value added of sector p at time t.
$\alpha_p(t)$	Variable	Overproduction capacity as the ratio to the pre-disaster production level of sector p at time t.
α_p^{max}	Parameter	Maximum overproduction capacity of sector$p$.
τ_p^{α}	Parameter	Time to achieve maximum overproduction capacity of sector$p$.
τ_p^s	Parameter	Time of inventory restoration of sector p.
η_p	Parameter	Target inventory level of supplying sector p in days of demand.
ψ_p	Parameter	Heterogeneity parameter of sector p.

Table 3. Economic behavioral parameters for various categories of economic sectors (taken as the mean values suggested in [35]). The construction sector does not have an inventory constraint, so inventory parameters are labeled as n.a. in the table and set to infinity in the model.

Category	α^{max}	τ^{α} (months)	τ^s (days)	η (days)	ψ
Agriculture, forestry and fishery	1.1	12	30	90	0.7
Mining	1.1	12	30	90	0.7
Beverages and Foods	1.1	6	30	90	0.7
Manufacturing	1.1	6	30	90	0.7
Construction	1.1	12	n.a.	n.a.	0.7
Utilities	1.1	0.5	2	2	0.7
Services	1.1	1	14	30	0.7

8.2. Building occupancy-to-industry mapping

Table 4 presents the mapping from HAZUS building occupancy classes to housing and 15 BEA sectors based on the HayWired mapping scheme [46] and established crosswalks between IMPLAN industries and NAICS classifications.

Table 4. Mapping of HAZUS building occupancy classes to housing and economic sectors. The share column gives the fractional allocation of each occupancy class to the listed sector.

HAZUS building occupancy class	Economic sector	Share
RES1	Housing	1.00
RES2	Housing	1.00
RES3	Housing	1.00
RES4	Arts, entertainment, recreation, accommodation & food	1.00
RES6	Educational services, health care & social	1.00
COM1	Retail trade	1.00
COM2	Wholesale trade	0.50
	Transportation & warehousing	0.50
COM3	Educational services, health care & social	0.33
	Arts, entertainment, recreation, accommodation & food	0.67
COM4	Utilities	0.17
	Transportation & warehousing	0.33
	Information	0.28
	Finance, insurance, real estate, rental & leasing	0.06
	Professional & business services	0.17
COM5	Finance, insurance, real estate, rental & leasing	1.00
COM6	Educational services, health care & social	1.00
COM7	Educational services, health care & social	1.00
COM8	Information	0.50
	Arts, entertainment, recreation, accommodation & food	0.50
IND1	Manufacturing	1.00
IND2	Manufacturing	0.50
	Information	0.50
IND3	Manufacturing	1.00
IND4	Mining	0.75
	Manufacturing	0.25
IND5	Manufacturing	1.00
IND6	Construction	1.00
AGR1	Agriculture, forestry, fishing & hunting	1.00
REL1	Other services, except government	1.00
GOV1	Government	1.00

Continued on next page.

Table 4 – continued from previous page.

HAZUS class	Economic sector	Share
GOV2	Government	1.00
EDU1	Educational services, health care & social	1.00
EDU2	Educational services, health care & social	1.00

8.3. Sector-level economic impacts for all sectors

Figure 14 and Figure 15 present the sector-level value added trajectories for all sectors under different model variants for road network disruptions and port disruptions, respectively.

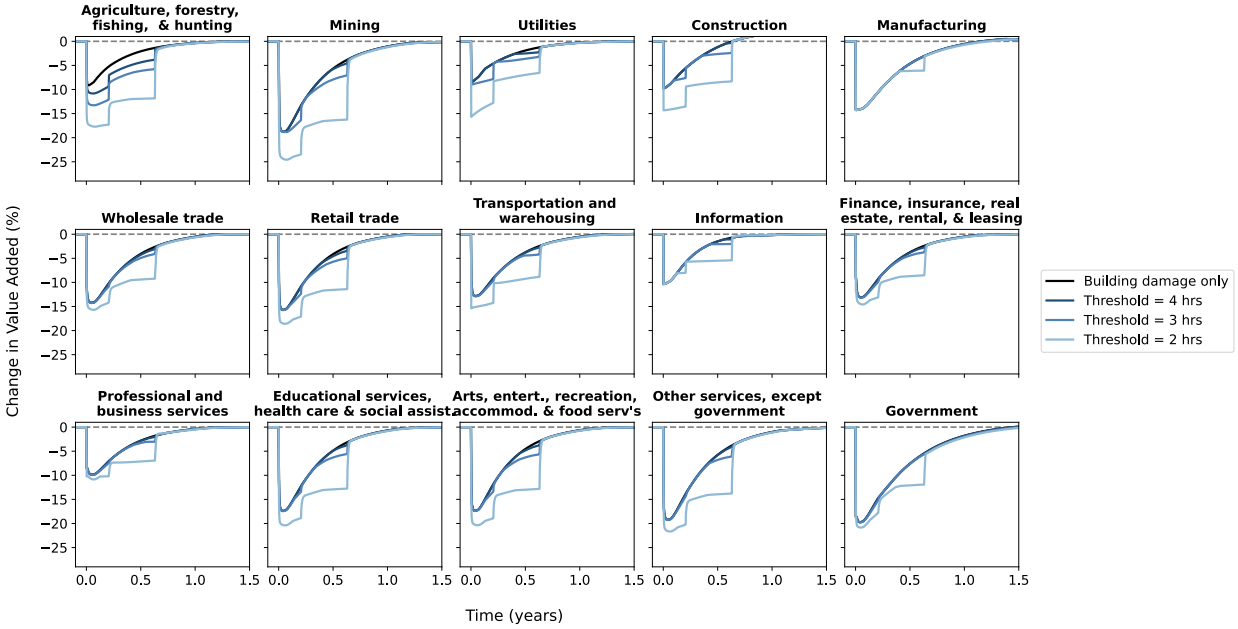


Fig. 14. Sectoral value added trajectory after the earthquake: R-ARIO model integrated with road network disruption for all 15 BEA sectors.

References

[1] C. Colon, S. Hallegatte, J. Rozenberg, Criticality analysis of a country's transport network via an agent-based supply chain model, Nature Sustainability 4 (3) (2021) 209–215.

[2] P. Gordon, H. W. Richardson, B. Davis, Transport-related impacts of the northridge earthquake, Journal of Transportation and Statistics 1 (2) (1998) 21–36.

[3] S. E. Chang, Disasters and transport systems: loss, recovery and competition at the port of kobe after the 1995 earthquake, Journal of transport geography 8 (1) (2000) 53–65.

[4] S. Giovinazzi, T. Wilson, C. Davis, D. Bristow, M. Gallagher, A. Schofield, M. Villemure, J. Eidinger, A. Tang, Lifelines performance and management following the 22 february 2011 christchurch earthquake, new zealand: highlights of resilience (2011).

[5] S. E. Chang, Socioeconomic impacts of infrastructure disruptions, in: Oxford research encyclopedia of natural hazard science, 2016.

[6] R. Nair, H. Avetisyan, E. Miller-Hooks, Resilience framework for ports and other intermodal components, Transportation Research Record 2166 (1) (2010) 54–65.

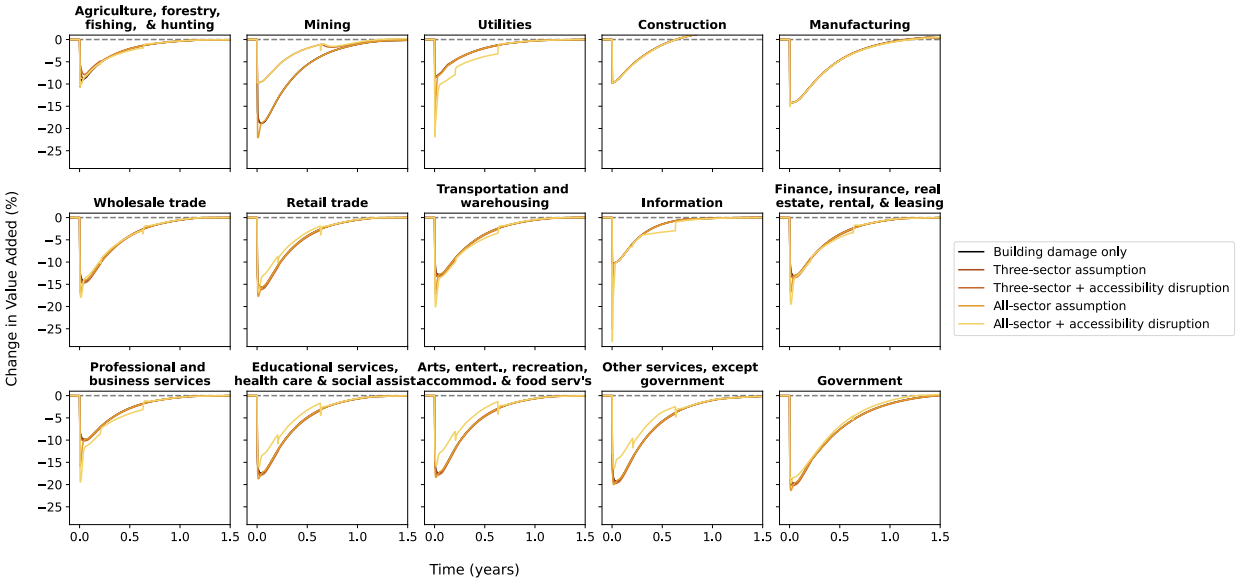


Fig. 15. Sectoral value added trajectory after the earthquake: R-ARIO model integrated with port disruption for all 15 BEA sectors.

[7] A. Tafur, J. E. Padgett, A flow-based commodity-independent port capacity model for resilience assessment of intermodal freight networks subjected to coastal hazards, Reliability Engineering & System Safety 250 (2024) 110280.

[8] D. Pachakis, A. S. Kiremidjian, Estimation of downtime-related revenue losses in seaports following scenario earthquakes, Earthquake Spectra 20 (2) (2004) 427–449.

[9] L. I. Burden, G. Rix, S. Werner, Development of a risk framework for forecasting earthquake losses in port systems, Earthquake Spectra 32 (1) (2016) 267–284.

[10] R. Faturechi, E. Miller-Hooks, Measuring the performance of transportation infrastructure systems in disasters: A comprehensive review, Journal of infrastructure systems 21 (1) (2015) 04014025.

[11] Y. Zhou, S. Banerjee, M. Shinozuka, Socio-economic effect of seismic retrofit of bridges for highway transportation networks: a pilot study, Structure and Infrastructure Engineering 6 (1-2) (2010) 145–157.

[12] B. Postance, J. Hillier, T. Dijkstra, N. Dixon, Extending natural hazard impacts: an assessment of landslide disruptions on a national road transportation network, Environmental Research Letters 12 (1) (2017) 014010.

[13] R. Silva-Lopez, G. Bhattacharjee, A. Poulos, J. W. Baker, Commuter welfare-based probabilistic seismic risk assessment of regional road networks, Reliability Engineering & System Safety 227 (2022) 108730.

[14] J. Boakye, R. Guidotti, P. Gardoni, C. Murphy, The role of transportation infrastructure on the impact of natural hazards on communities, Reliability Engineering & System Safety 219 (2022) 108184.

[15] S. Cho, P. Gordon, J. E. Moore II, H. W. Richardson, M. Shinozuka, S. Chang, Integrating transportation network and regional economic models to estimate the costs of a large urban earthquake, Journal of Regional Science 41 (1) (2001) 39–65.

[16] P. Gordon, J. E. Moore, H. W. Richardson, M. Shinozuka, D. An, S. Cho, Earthquake Disaster Mitigation for Urban Transportation Systems: An Integrated Methodology that Builds on the Kobe and Northridge Experiences, Springer Berlin Heidelberg, Berlin, Heidelberg, 2004, pp. 205–232.

[17] J. Sohn, T. J. Kim, G. J. D. Hewings, J. S. Lee, S.-G. Jang, Retrofit priority of transport network links under an earthquake, Journal of Urban Planning and Development 129 (4) (2003) 195–210.

[18] F. Wei, E. Koc, L. Soibelman, N. Li, Disturbances to urban mobility and comprehensive estimation of economic losses, Polytechnica 1 (2018) 48–60.

[19] E. Koc, B. Cetiner, A. Rose, L. Soibelman, E. Taciroglu, D. Wei, Craft: Comprehensive resilience assessment framework for transportation systems in urban areas, Advanced Engineering Informatics 46 (2020) 101159.

[20] D. Wei, A. Rose, E. Koc, Z. Chen, L. Soibelman, Socioeconomic impacts of resilience to seaport and highway transportation network disruption, Transportation Research Part D: Transport and Environment 106 (2022) 103236.

[21] L. A. Tavasszy, M. Thissen, J. Oosterhaven, Challenges in the application of spatial computable general equilibrium models for transport appraisal, Research in Transportation Economics 31 (1) (2011) 12–18.

[22] A. Rose, Economic principles, issues, and research priorities in hazard loss estimation, in: Y. Okuyama, S. E. Chang (Eds.),

Modeling Spatial and Economic Impacts of Disasters, Springer Berlin Heidelberg, Berlin, Heidelberg, 2004, pp. 13–36.
[23] N. J. McDonald, G. W. McDonald, Towards a dynamic equilibrium-seeking model of a closed economy, Systems 8 (4) (2020) 42.
[24] C. Brown, N. McDonald, G. McDonald, M. Daly, E. Seville, Using an integrated dynamic economic model to support infrastructure investment decision-making, Earthquake Spectra 39 (4) (2023).
[25] J. Fu, E. Jenelius, Transport efficiency of off-peak urban goods deliveries: A stockholm pilot study, Case Studies on Transport Policy 6 (1) (2018) 156–166.
[26] K. K. Hyun, S. P. Mattingly, M. Arabi, The impacts of increased adverse weather events on freight movement, Tech. rep., Transportation Consortium of South-Central States (2020).
[27] S. Hallegatte, An adaptive regional input-output model and its application to the assessment of the economic cost of katrina, Risk Analysis: An International Journal 28 (3) (2008) 779–799.
[28] M. Markhvida, B. Walsh, S. Hallegatte, J. Baker, Quantification of disaster impacts through household well-being losses, Nature Sustainability 3 (7) (2020) 538–547.
[29] M. Yashinsky, The Loma Prieta, California, Earthquake of October 17, 1989, Highway Systems, no. 1552, US Government Printing Office, 1998.
[30] N. I. Basöz, A. S. Kiremidjian, S. A. King, K. H. Law, Statistical analysis of bridge damage data from the 1994 northridge, ca, earthquake, Earthquake spectra 15 (1) (1999) 25–54.
[31] Y. Dong, D. M. Frangopol, D. Saydam, Sustainability of highway bridge networks under seismic hazard, Journal of Earthquake Engineering 18 (1) (2014) 41–66.
[32] A. M. Wein, J. L. Jones, L. A. Johnson, C. Kroll, J. A. Strauss, D. Witkowski, D. A. Cox, The Haywired earthquake scenario—societal consequences, US Geological Survey (2021).
[33] K. T. Geurs, B. Van Wee, Accessibility evaluation of land-use and transport strategies: review and research directions, Journal of Transport geography 12 (2) (2004) 127–140.
[34] S. Fotopoulou, S. Karafagka, A. Karatzetzou, K. Pitilakis, System-wide seismic risk assessment of port facilities; application to the port of thessaloniki, greece, Sustainability 14 (3) (2022) 1424.
[35] O. Issa, T. Zhu, M. Markhvida, R. Costa, J. W. Baker, Refined adaptive regional input–output model: Application to the 2016 kumamoto earthquake, Natural Hazards Review 26 (4) (2025) 04025050.
[36] E. H. Field, G. P. Biasi, P. Bird, T. E. Dawson, K. R. Felzer, D. D. Jackson, K. M. Johnson, T. H. Jordan, C. Madden, A. J. Michael, et al., Long-term time-dependent probabilities for the third Uniform California Earthquake Rupture Forecast (UCERF3), Bulletin of the Seismological Society of America 105 (2A) (2015) 511–543.
[37] M. D. Petersen, M. Moschetti, P. Powers, C. Mueller, K. Haller, A. Frankel, Y. Zeng, S. Rezaeian, S. Harmsen, O. Boyd, et al., Documentation for the 2014 update of the United States national seismic hazard maps: US Geological Survey Open-File Report 2014–1091 (2014).
[38] C. B. Worden, E. M. Thompson, M. Hearne, D. J. Wald, Shakemap manual online: Technical manual, user's guide, and software guide, US Geological Survey (2020).
[39] F. McKenna, S. Gavrilovic, J. Zhao, K. Zhong, A. Zsarnoczay, B. Cetiner, S. Naeimi, S.-r. Yi, A. B. Satish, P. Arduino, W. Elhaddad, NHERI-SimCenter/R2DTool: Version 5.3.0 (v5.3.0), Zenodo (2025).
[40] M. Largent, J. Bray, J. Watson-Lamprey, N. Abrahamson, Developing software to assess the seismic risk of natural gas infrastructure: Opensra, Frontiers in Built Environment 9 (2023) 1176919.
[41] G. G. Deierlein, F. McKenna, A. Zsarnóczay, T. Kijewski-Correa, A. Kareem, W. Elhaddad, L. Lowes, M. J. Schoettler, S. Govindjee, A cloud-enabled application framework for simulating regional-scale impacts of natural hazards on the built environment, Frontiers in Built Environment 6 (2020) 558706.
[42] B. Cetiner, C. Wang, F. McKenna, S. Hornauer, J. Zhao, Y. Guo, S. X. Yu, E. Taciroglu, K. H. Law, NHERI-SimCenter/BRAILS: Version v3.1.1 (2024). doi:10.5281/zenodo.10606032.
[43] Federal Emergency Management Agency (FEMA), Hazus earthquake model technical manual: Hazus 5.1, Tech. rep., Federal Emergency Management Agency (FEMA), Washington, D.C. (2023).
[44] A. Zsarnoczay, J. V. Manousakis, J. Zhao, NHERI-SimCenter/pelicun (2025). doi:10.5281/zenodo.17217508.
[45] E. M. Rathje, C. Dawson, J. E. Padgett, J.-P. Pinelli, D. Stanzione, A. Adair, P. Arduino, S. J. Brandenberg, T. Cockerill, C. Dey, M. Esteva, F. L. Haan, M. Hanlon, A. Kareem, L. Lowes, S. Mock, G. Mosqueda, Designsafe: A new cyberinfrastructure for natural hazards engineering, Natural Hazards Review 18 (2) (2017) 06017001.
[46] I. Sue Wing, D. Wei, A. Z. Rose, A. M. Wein, Economic consequences of the haywired earthquake scenario, in: Lifelines 2022, 2022, pp. 523–533.
[47] M. K. Miller, Seismic risk assessment of complex transportation networks, Ph.D. thesis, Stanford University (2014).
[48] M. Beckmann, C. B. McGuire, C. B. Winsten, Studies in the economics of transportation, 1956.
[49] Y. Bai, W. R. Burkett, P. T. Nash, Rapid bridge replacement under emergency situation: Case study, Journal of Bridge Engineering 11 (3) (2006) 266–273.

[50] National Academies of Sciences, Engineering, and Medicine, Response Planning, Assessment, and Rapid Restoration of Service of Bridges in Extreme Events: Background and Summary, The National Academies Press, Washington, DC, 2024.
[51] R. Fabling, A. Grimes, L. Timar, Labour market dynamics following a regional disaster, Tech. rep., Motu Economic and Public Policy Research (2016).
[52] Y. Cui, D. Liang, B. Ewing, Analysis of employment change in response to hurricane landfalls, Natural Hazards and Earth System Sciences Discussions 2019 (2019) 1–16.
[53] U.S. Bureau of Labor Statistics, Labor Force Statistics from the Current Population Survey, Table 42. People at work by telework status, usual full- or part-time status, occupation, industry, and class of worker (2022).
[54] U.S. Census Bureau, Means of transportation to work, american Community Survey, Table B08301 (2024).
[55] S. T. Detweiler, A. M. Wein, The HayWired earthquake scenario—engineering implications, US Geological Survey (2021).
[56] U.S. Army Corps of Engineers, Waterborne commerce of the United States, 2022.
[57] J. Verschuur, E. Koks, J. Hall, Port disruptions due to natural disasters: Insights into port and logistics resilience, Transportation research part D: transport and environment 85 (2020) 102393.
[58] T. Zhu, O. Issa, M. Markhvida, R. Costa, J. W. Baker, Multi-regional economic recovery simulation using an adaptive regional input–output (ario) framework, International Journal of Disaster Risk Reduction 112 (2024) 104766.
[59] B. Marion, M. W. Horner, Comparison of socioeconomic and demographic profiles of extreme commuters in several us metropolitan statistical areas, transportation research record 2013 (1) (2007) 38–45.